



**UNIVERSIDAD DE INVESTIGACIÓN DE TECNOLOGÍA
EXPERIMENTAL YACHAY**

Escuela de Ciencias de la Tierra, Energía y Ambiente

**RECONSTRUCCIÓN CLIMATOLÓGICA DE LA INUNDACIÓN
DE ENERO DE 2016 EN ESMERALDAS**

Trabajo de integración curricular presentado como requisito para la
obtención del título de Geólogo

Autor:

Juan Andres Changoluisa Segovia

Tutor:

Ph.D. Luis Eduardo Pineda Ordoñez

Urcuquí, Febrero 2020

SECRETARÍA GENERAL
(Vicerrectorado Académico/Cancillería)
ESCUELA DE CIENCIAS DE LA TIERRA, ENERGÍA Y AMBIENTE
CARRERA DE GEOLOGÍA
ACTA DE DEFENSA No. UITEY-GEO-2020-00005-AD

A los 18 días del mes de marzo de 2020, a las 11:30 horas, de manera virtual mediante videoconferencia, y ante el Tribunal Calificador, integrado por los docentes:

Presidente Tribunal de Defensa	Mgs. SOLIS AULESTIA, MARIA JOSE
Miembro No Tutor	Mgs. FLORES DE LA TORRE, JOSE LUIS
Tutor	Dr. PINEDA ORDOÑEZ, LUIS EDUARDO , Ph.D.

El(la) señor(ita) estudiante **CHANGOLUISA SEGOVIA, JUAN ANDRES**, con cédula de identidad No. **0503969446**, de la **ESCUELA DE CIENCIAS DE LA TIERRA, ENERGÍA Y AMBIENTE**, de la Carrera de **GEOLOGÍA**, aprobada por el Consejo de Educación Superior (CES), mediante Resolución **RPC-SE-10-No.031-2016**, realiza a través de videoconferencia, la sustentación de su trabajo de titulación denominado: **CLIMATOLOGICAL RECONSTRUCTION OF JANUARY 2016 FLOOD IN ESMERALDAS**, previa a la obtención del título de **GEÓLOGO/A**.

El citado trabajo de titulación, fue debidamente aprobado por el(los) docente(s):

Tutor	Dr. PINEDA ORDOÑEZ, LUIS EDUARDO , Ph.D.
--------------	--

Y recibió las observaciones de los otros miembros del Tribunal Calificador, las mismas que han sido incorporadas por el(la) estudiante.

Previamente cumplidos los requisitos legales y reglamentarios, el trabajo de titulación fue sustentado por el(la) estudiante y examinado por los miembros del Tribunal Calificador. Escuchada la sustentación del trabajo de titulación a través de videoconferencia, que integró la exposición de el(la) estudiante sobre el contenido de la misma y las preguntas formuladas por los miembros del Tribunal, se califica la sustentación del trabajo de titulación con las siguientes calificaciones:

Tipo	Docente	Calificación
Presidente Tribunal De Defensa	Mgs. SOLIS AULESTIA, MARIA JOSE	8,8
Tutor	Dr. PINEDA ORDOÑEZ, LUIS EDUARDO , Ph.D.	9,7
Miembro Tribunal De Defensa	Mgs. FLORES DE LA TORRE, JOSE LUIS	9,1

Lo que da un promedio de: **9.2 (Nueve punto Dos)**, sobre 10 (diez), equivalente a: **APROBADO**

Para constancia de lo actuado, firman los miembros del Tribunal Calificador, el/la estudiante y el/la secretario ad-hoc.

CHANGOLUISA SEGOVIA, JUAN ANDRES
Estudiante

 Firmado electrónicamente por:
MARIA JOSE
SOLIS

Mgs. SOLIS AULESTIA, MARIA JOSE
Presidente Tribunal de Defensa

Dr. PINEDA ORDOÑEZ, LUIS EDUARDO , Ph.D.
Tutor

 Firmado electrónicamente por:
LUIS EDUARDO
PINEDA
ORDONEZ

 Firmado electrónicamente por:
JOSE LUIS
FLORES DE LA
TORRE
Mgs. FLORES DE LA TORRE, JOSE LUIS
Miembro No Tutor

ANDREA
YOLANDA
TERAN ROSALES

Firmado digitalmente
por ANDREA YOLANDA
TERAN ROSALES
Fecha: 2020.03.26
11:31:20 -0500'

TERÁN ROSALES, ANDREA YOLANDA
Secretario Ad-hoc

AUTORÍA

Yo, **Juan Andrés Changoluisa Segovia**, con cédula de identidad 0503969446, declaro que las ideas, juicios, valoraciones, interpretaciones, consultas bibliográficas, definiciones y conceptualizaciones expuestas en el presente trabajo; así cómo, los procedimientos y herramientas utilizadas en la investigación, son de absoluta responsabilidad de el/la autora (a) del trabajo de integración curricular. Así mismo, me acojo a los reglamentos internos de la Universidad de Investigación de Tecnología Experimental Yachay.

Urcuquí, Marzo 2020.



Juan Andres Changoluisa Segovia

CI: 0503969446

AUTORIZACIÓN DE PUBLICACIÓN

Yo, **Juan Andres Changoluisa Segovia**, con cédula de identidad 0503969446, cedo a la Universidad de Tecnología Experimental Yachay, los derechos de publicación de la presente obra, sin que deba haber un reconocimiento económico por este concepto. Declaro además que el texto del presente trabajo de titulación no podrá ser cedido a ninguna empresa editorial para su publicación u otros fines, sin contar previamente con la autorización escrita de la Universidad.

Asimismo, autorizo a la Universidad que realice la digitalización y publicación de este trabajo de integración curricular en el repositorio virtual, de conformidad a lo dispuesto en el Art. 144 de la Ley Orgánica de Educación Superior

Urcuquí, Marzo 2020.



Juan Andres Changoluisa Segovia

CI: 0503969446

DEDICATORIA

A mis padres, Juan y Rosa, el soporte de mi vida, mis hermanos, Juan Pablo y Lucía

Y a todas las personas que me han apoyado incondicionalmente.

Juan Andres Changoluisa Segovia

RESUMEN

Ecuador es un país propenso a inundaciones, particularmente la región costera experimenta inundaciones debido a su topografía y variaciones climáticas interanuales, pero hay algunos eventos que exceden las condiciones de inundación esperadas en los registros históricos, como fue el caso del evento del 25 de enero de 2016 en la provincia de Esmeraldas. El evento de alta precipitación (EAP) que azotó una gran parte de la provincia durante más de 12 horas dejó una víctima en Mataje (cantón San Lorenzo), 140 familias evacuadas debido a la inundación de los ríos Esmeraldas, Teone, Súa, Santiago, Ónzole, Mataje y muchos asentamientos en el norte de Esmeraldas aislados. Este estudio se centra en el análisis climatológico y la reconstrucción de este EAP sobre la cuenca del río Esmeraldas. Mediante el uso de productos de imágenes satelitales, registros instrumentales de precipitación y análisis retrospectivos de modelos climáticos se reconstruyeron las condiciones atmosféricas que condujeron a la ocurrencia de precipitaciones de alta intensidad y gran escala.

El primer objetivo fue preparar un atlas de hietogramas y mapas de contornos que describan las características de la lluvia diaria durante el evento de clima extremo utilizando datos de pluviómetros e imágenes satelitales para obtener información sobre el tipo, tamaño y la duración de la tormenta. En segundo lugar, se analizó la relación entre las condiciones atmosféricas y el EAP utilizando vientos horizontales y humedad específica en la atmósfera de bajo nivel para revisar las condiciones meteorológicas que conducen al pulso de inundación. Específicamente, los patrones de circulación atmosférica que acompañan al EAP en comparación con las condiciones normales de la sub temporada entre Diciembre-Febrero.

Se descubrió que el EAP pertenece a la categoría de sistemas convectivos de mesoescala, específicamente un complejo convectivo de mesoescala (CCM). El tamaño de la escala del sistema de lluvia intensa fue meso- β (~ 250 km), con un ciclo de vida de 16 horas para la tormenta completa con 6 horas de lluvias convectivas. La génesis del CCM probablemente estuvo relacionada con condiciones de humedad superficial por encima de lo normal y el levantamiento orográfico que impulsó corrientes ascendentes convectivas forzadas por la barrera montañosa N-S. Esta cadena montañosa actuó en dos formas, aumentando el flujo de la pendiente ascendente cuando se mueve sobre laderas, y también como refugio de lluvia intensa para los valles interiores que recibieron solo precipitación de nubes estratiformes. En cuanto a los vientos, se mostró un cizallamiento moderado de bajo nivel hacia el oeste con una velocidad de viento de aproximadamente 10 m/s, en la etapa de disipación este flujo alejó el aire inestable y el patrón convectivo desapareció sobre la línea de costa de la cuenca del Esmeraldas.

En conclusión, este estudio contribuye a llenar la falta de información sobre los eventos de alta precipitación en el noroeste de América del Sur, lo que debería ayudar a comprender su dinámica e informar sobre su potencial previsibilidad.

Palabras Clave: Reconstrucción climatológica, evento de alta precipitación, imágenes satelitales, sistema convectivo de mesoescala.

ABSTRACT

Ecuador is a country prone to floods, particularly the coastal region experiences flooding due to its topography and inter-annual climate variations, but there are some events that exceed the expected long-term flood conditions, as it was the case of the 25th January 2016 event in the Esmeraldas province. The high precipitation event (HPE) that hit a large part of the province for more than 12 hours left one casualty in Mataje (canton San Lorenzo), 140 families evacuated because the flooding of Esmeraldas, Teaone, Súa, Santiago, Ónzole and Mataje rivers, and many settlements in northern Esmeraldas isolated. This study focuses on the climatological analysis and reconstruction of this HPE over the Esmeraldas river basin. By using satellite images and products, gauge data and retrospective climate model analysis, the atmospheric conditions leading to the occurrence of high intensity and wide-spread heavy precipitation were reconstructed.

The first goal was to prepare an atlas of hietograms and contour maps describing daily rainfall characteristics during the extreme weather event using rainfall gauge data and satellite imagery in order to obtain information on type, size, and duration of the storm. Secondly, the relationship between the atmospheric conditions and the HPE was analyzed using horizontal winds and specific humidity at the low-level atmosphere in order to revisit the meteorological conditions leading to the flood pulse. Specifically, the atmospheric circulation patterns that accompany the HPE as compared with the normal conditions of the December-February sub-season.

It was found that the HPE belongs to the Mesoscale Convective Systems category, specifically a Mesoscale Convective Complex (MCC). The scale size of the heavy rainfall system was meso- β (~250 km) with a lifecycle lasting 16 hours for the complete storm with 6 hours of convective showers. The genesis of the MCC was likely above normal moisture and orographic lifting driving convective updrafts which are further enhancement by the N-S mountain barrier. This mountain range acted as both channels to boost upslope flow when it moves over hillslopes, and also as rain shelter for the inner valleys that received only stratiform precipitation. The wind environment showed moderate low-level easterly shear with wind velocity of about 10 m/s, in the dissipation stage this flow moved away the unstable air and the convective pattern disappear on the shore of the Esmeraldas basin.

In conclusion, this study contributes to fill the lack of information of heavy precipitation events in north-western South America, which should help to understand its dynamics and shed light on its potential predictability.

Key Words: Climatological reconstruction, high precipitation event, satellite imagery, mesoscale convective system.

This undergraduate thesis has been approved in partial fulfillment of the requirements for the Degree of BACHELOR OF SCIENCE in Geology.

Thesis Advisor: Luis Eduardo Pineda Ordoñez, Ph.D.
School of Earth Sciences, Energy and Environment

Committee Member: José Luis Flores De La Torre, M.Sc.

Committee Member: María José Solis Aulestia, Ph.D.

CONTENT

1. INTRODUCTION.....	1
2. PROBLEM STATEMENT	2
3. OBJECTIVES	3
4. STUDY AREA.....	3
4.1 Climate of Ecuador	3
4.2 The annual cycle of precipitation in coastal Ecuador.....	4
4.3 Tropical Mesoscale Convective Systems	5
4.3.1 Structure.....	7
4.3.2 Types.....	10
4.2.2.1 Non-squall Tropical Clusters	10
4.3.2.2 Mesoscale Convective Complexes	11
4.3.2.3 Squall Clusters/Lines	11
4.3.2.3.1 Bow Echoes	11
4.3.2.4 Mesoscale convective Vortices.....	12
4.4 Esmeraldas river basin	12
4.5 The January 2016 flood	13
5. MATERIALS AND METHODS	16
5.1 Hydrometeorological characterization	16
5.2 Precipitation and river flow data.....	17
5.3 Wind circulation:	18

5.3.1 National Centers for Environmental Prediction (NCEP) and the National Center for Atmospheric Research (NCAR) Reanalysis	18
5.4 Satellite imagery:	19
5.4.1 Geostationary Operational Environmental Satellites	19
5.4.2 Climate Hazards group Infrared Precipitation with Stations	21
5.4.3 Tropical Rainfall Mission Measurement 3B42.....	21
5.5 Spatial fields of precipitation:	22
5.5.1 Mean Bias Correction	22
5.5.2 Double-Kernel Smoothing.....	22
5.5.3 Ordinary Kriging.....	24
5.5.4 Kriging with External Drift.....	24
6. RESULTS AND DISCUSSION	25
6.1 Storm properties	25
6.1.1 Life span.....	25
6.1.2 Area.....	26
6.2 Precipitation	28
6.3 Climatological Analysis	31
6.4 The January 2016 HPE	37
7. SUMMARY AND CONCLUSIONS	41
9. ACKNOWLEDGEMENTS	44
10. BIBLIOGRAPHY	45
11. ANNEXES	49

TABLE OF FIGURES

Figure 1. Climatology of Mesoscale Convective Systems in January measured by a Special Sensor Microwave/Imager (SSM/I) 85 GHz Minimum Polarization Corrected Temperature. a) sunrise passes b) sunset passes (Mohr and Zipser, 1986).	6
Figure 2. Climatology of Mesoscale Convective Systems in April measured by a Special Sensor Microwave/Imager (SSM/I) 85 GHz Minimum Polarization Corrected Temperature. a) sunrise passes b) sunset passes (Mohr and Zipser, 1986).	7
Figure 3. The dynamic structure of MCCs: Updrafts (Morrison et al., 2012).	8
Figure 4. The dynamic structure of MCCs: Stratiform precipitation area (Morrison et al., 2012).	8
Figure 5. The dynamic structure of MCCs: Enhanced updraft due to feedback mechanisms (Morrison et al., 2012).	9
Figure 6. Schematic of the structure of deep convection over a) Central Africa and b) the northwestern tropical Pacific, demonstrating differences between typical strong systems in the two regions (Liu et al., 2007).	10
Figure 7. Study area showing INAMHI hydrological stations (white circles) and the main rivers in the Esmeraldas basin (blue lines). H0172 (Teaone) and H0177 (Quinindé)	13
Figure 8. a) Water level in station Teaone (H0172). Broken-line window shows January 2016. b) Average catchment station precipitation upstream station (H0177). c) River discharge in station Quinindé (H0177) in January 2016.	14
Figure 9. Empirical return period (years) vs monthly maxima precipitation (mm) in January for the 1987-2018 period in selected meteorological stations. (Dots) with trend line (dashed-line). Horizontal lines show the January 2016 event (red) and the 2002 and 1997 ENSO events. a) Apuela-Intag (M0318), b) Chontal Bajo (M0327), c) San José de Minas (M0337) and d) Santa Anita (M0348).	15
Figure 10. Development of the storm cloud during the event day (25/01/2016) as observed via satellite GOES 13.	27
Figure 11. Daily precipitation (mm) retrieved from INAMHI stations during a) 24 th , c) 25 th and c) 26 th of January 2016.	29

Figure 12. a) Daily mean precipitation estimated by satellite (SAT), and interpolated by DS, KED and MBC techniques for the 25-01-2016. b) The percent bias % between the rain gauge time series and merging product at all cross-validation points. 30

Figure 13. HMM state anomaly composites of horizontal winds (vectors) and specific humidity at 850 hPa (colors) with respect to December- February climatology for 1964-2010 (a)-(d) state 1-4 respectively. 33

Figure 14. a) Viterbi sequence of most likely states 1964-2010 b) Climatology for each day during 46 years period. Colors represents states 1-4..... 34

Figure 15. Climatological analysis for the period 20th – 30th January 2016 using horizontal winds (vectors) and specific humidity at 850 hPa (colors). 36

Figure 16. 3D terrain model based on Shuttle Radar Topography Mission (SRTM-dem) of Esmeraldas basin (red line) showing meteorological stations and precipitation on 25th of January 2016 (red-wine dots). The vertical scale is exaggerated 0.5x. 39

Figure 17. 3D terrain model of Esmeraldas river basin (red line) overlapped by TRMM precipitation data for a time sequence of storm events recorded every 3 hours within 24th-25th January 2016. The sequence starts at 24th Januray at 22:30. 40

INDEX OF TABLES

Table 1. Meteorological stations with daily precipitation data for the period 1985-2018 divided by sub-basins..... 17

Table 2. Detailed information of satellite imagery retrieved from CLASS system. 20

Table 3. Cloud area measured by satellite imagery using longwave IR window (band 4) from GOES 13. 25

Table 4. Climatological characteristics of study event, genesis, wind shear, propagation and dissipation. 39

1. INTRODUCTION

The coastal region of Ecuador is characterized by large inter-annual climatic variations (Cruz et al., 1979). Normal and dry-year periods are interrupted by years with abundant rainfall and flooding. Such rainfall anomalies are related to above normal conditions in the ocean-atmospheric circulation inland and offshore Ecuador. The section of the ocean off Ecuador, where the cold Humboldt Current meets the warm equatorial current, is a key region for development of the El Niño/Southern Oscillation (ENSO) phenomenon (Rasmusson and Carpenter, 1982). The impact of this climatic anomaly is very important in the Ecuadorian coastal area. Sea warming associated with the ENSO, usually, results in abnormal precipitations and floods, which may cause considerable material and human losses. This was the situation in Ecuador and North Peru in the 1983 rainy season, which caused the death of at least 600 people (CEPAL, 1983). The situation recurred in 1998 with dramatic losses of human lives and infrastructure. The low relief and poor drainage of the coastal plains exacerbate the impact of the flooding (Rossel and Cadier, 2009).

In the 21st century the relation between El Niño and heavy rainfall in coastal Ecuador is less clear, the El Niño event 2010 did not result in massive flooding over coastal Ecuador (Bendix et al., 2011), however the El Niño event 2015/2016 led to unprecedented torrential precipitation over the northern coast of Ecuador. Northern Ecuador, in particular the Province of Esmeraldas was affected by heavy and long-lasting rainfall between 24th and 25th January (2016) triggering floods and landslides so that at least 2 out of the 7 cantons of the province declared an emergency. According to a report made by the Ecuador's Risk Management Secretariat (Secretaría de Gestión de Riesgo or SGR, its acronym in Spanish), a mesoscale convective system developed in the coastal region, with significant records of rainfall in 24 hours. The rain gauge station in Esmeraldas, the Province's capital city, recorded 244.5 mm in 24 hours, while Muisne (50 km west) recorded 88.5 mm. The rainfall intensified at around 23:00 on 24th January and lasted through the night, causing severe flooding by early 25th January. Several rivers overflowed, including the Teaone River in Esmeraldas and Atacames, the Blanco and Quinindé Rivers in Quinindé, and the Santiago River in Eloy Alfaro, causing major damages to the population living near the river banks.

While the dynamics of the atmospheric circulation and its relation with heavy storm formation during the mega El Niño events of 1983 and 1997 is fairly well documented (Goldberg et al., 1987;

Waylen et al., 1987; Bendix and Bendix, 2006), little is still known on the prevailing climatic conditions, the atmospheric dynamics and the characteristics of the heavy storms during the last mega El Niño, the 2015/2016 event. This latter is important for understanding the underlying mechanism leading to recent widespread and devastating flooding over coastal Ecuador in the context of a changing climate as well as to set the physical basis for its predictability.

2. PROBLEM STATEMENT

The rainy season in coastal Ecuador is characterized by large rainfall volumes within December-May. They often peak in February-April as a response to the maxima of atmospheric precipitable water vapor available off and on shore coastal Ecuador. This is the result of the annual offshore moisture supply, which is driven by the climatological maximum of sea surface temperatures (SSTs) in the El Niño-1.2 region in December-February. Other important components are moisture imports driven by large-scale atmospheric circulation, associated with the annual displacement of the Inter-tropical Convergence Zone (ITCZ). The timing and distribution of this moisture over the western slope of the Andes determines catchment seasonal rainfall regimes over coastal river basins in Ecuador, which vary from a fairly distributed regime in December-May on the north ($\sim 1^\circ\text{N}$) to one or two-month single rainy period over the southern coast of Ecuador ($\sim 5^\circ\text{S}$).

With regard heavy storm events, there is little information on the precipitation characteristics during the normal rainy season in coastal Ecuador as well as during extreme climatic episodes. Most of the literature has focused on storm analysis within El Niño episodes. For example, Bendix et al., (2006) studied the extreme episode of El Niño 1997/1998, using satellite imagery and rainfall estimates, and showed that the dynamics of heavy precipitation during the super El Niño 1997/98 was characterized by three mechanisms: (1) rainfall formation due to mesoscale thermal systems like the land-sea breeze phenomenon, (2) intensification of deep convection in the coastal plains by spill-over effects of cirrus remnants from the Amazon and (3) extended convection which is organized in Multi-scale Convective Complex (MCCs) in combination with anomalous westerly winds over the eastern Pacific. These results were in strong correspondence with previous studies of a normal El Niño 1991/92. In addition, Bendix and Bendix (2006) showed that high SSTs in combination with strong SST gradients off the coast and warm SST bubbles lead to regional differences in moist instability and heavy rainfall. Both large-scale circulation (reversal of the

Walker cell) and regional dynamics (extended land-sea-breeze system) have been proven to contribute to El Niño rainfall. It is, therefore, of both scientific and practical value to study whether the January 2016 heavy storm event over Esmeraldas, in the aftermath of El Niño 2015/2016 event showed the same characteristics as those attributed to heavy precipitation dynamics in coastal Ecuador during the past mega El Niño events. The characterization of heavy storms in terms of the physical mechanisms leading their development as well as the impacts on flood generation is an important step towards a storm type classification framework for Ecuador. At present, such classification framework, tailored for local climate conditions, is lacking in the synoptic and meso-scale meteorological literature, thus this study attempts being a first contribution to fill knowledge gaps and provide some basis for the predictability of extreme precipitation events.

3. OBJECTIVES

The main objective of the investigation is:

- To perform a climatological characterization of the January-2016 flood in Esmeraldas.

Objectives:

- To reconstruct the heavy precipitation dynamics during the extreme weather event using gauge data and satellite imagery over the Esmeraldas catchment.
- To investigate the atmospheric conditions (winds, atmospheric moisture transport) leading to heavy rainfall formation and its relation with the regional climate.

4. STUDY AREA

4.1 Climate of Ecuador

Ecuador is a country located in South America on the equatorial line and divided in three main climatic regions by the Andes. In general terms, the continental territory is composed by three regions: Coast, Inter-Andean valleys (Sierra) and Amazonia. Esmeraldas the target study area is located near to the Pacific Ocean on the northern part of the coastal region. The territory is plain,

showing small hills with a height of a maximum 30 masl. down to the coast. The Pacific Ocean, just in front of the coast of Ecuador, is the place where seasonally two main oceanic currents meet: from Guayaquil to the north, the warm equatorial El Niño current approaching the continent from the eastern Pacific, and the Humboldt current coming from the south of the continent.

At synoptic scale, the Andean mountains inside the country are the articulation between two world-scale acting pressure systems: the subtropical highs over the Atlantic Ocean and the subtropical highs over the Southeastern Pacific. Those systems lead the synoptic currents that acts in southern Ecuador almost during all the year. Specially, the mid-level layers act in the large westward movement across the equatorial South American continent and the Ecuadorian Andes. Therefrom, the Ecuadorian Andean mountain barrier constitutes a veritable division in the climate of the country.

The main factors that act in shaping the climate in Ecuador region are the oceanic anticyclones in the subtropical ridges, because they are the drivers of easterly trades. These trades help to keep the east part of the Ecuadorian mountains wet and hold the precipitation from Sierra approximately all the year. The subtropical anticyclones have its high levels on the southern and northern hemispheres in July-August and decrease on February. The excess of pressure on July-August over the tropical Atlantic zone causes the zonal pressure gradient between the two oceans, this could be considered the motor of the easterlies winds over equatorial South America (Emck, 2007).

4.2 The annual cycle of precipitation in coastal Ecuador

Throughout the year, the north-eastern trade winds emanating from the North Atlantic high sweep over the Caribbean Sea into northern South America and across the Central American land bridge into the eastern Pacific. The southern trade winds in conjunction with the South Pacific high follow the South American coast and the Andes Mountain before moving to the west under the influence of the Coriolis force. North and south trade winds meet along the inter-tropical convergence zone (ITCZ). The ITCZ is a band of maximum convergence, convection, cloudiness and rainfall. Southwards, very dry climatic conditions are established. Owing to such high latitudinal climatic gradients, a small ITCZ displacement results in a large modification of the local atmospheric state. The seasonal shift in the latitude of the ITCZ follows the sun. Over December-February, the north-eastern trade winds blow vigorously across the Central American Isthmus, whereas the southern

trade winds are weak. The ITCZ is then at its southernmost position near the equator. Over June-August, the South Pacific high migrates north-eastward, the South Pacific trade winds become stronger and the ITCZ reaches its northernmost position. When South Pacific trade winds go through the equator, a divergence appears, with the formation of monsoon winds blowing to the Gulf of Panama. Along the South America's west coast, the cold Humboldt Current (14–18°C) sweeps northward while the trade winds promote a cold water upwelling. This cold current meets the hot (>25°C) south equatorial current generally between North Peru and the Galapagos Islands. As such, water currents are combined with trade winds, the latitude of their convergence, called the equatorial front, follows the ITCZ movement.

Ecuador's coastal regions, where a strong ENSO influence exists, have a seasonal rainfall distribution characterized by a single rainy period, with 75–90% of the rainfall occurring between December and May. The rainy season starts around late November and ends in June, with a peak between February and March. The rainy season is separated from the next rainy season by a 2–6-months dry period. This seasonal distribution of rainfall in Ecuador's coastal region is combined with the seasonal latitudinal ITCZ migration and eastern tropical Pacific SST variations. The north-southern seasonal ITCZ displacement and SST variations bring to the area air masses of different humidity and temperature. When the ITCZ and the equatorial front are in their southernmost position near the equator, Ecuador's coastal regions are under the influence of warm moist air masses, which come from the northwest, and which bring significant rainfall and increase air temperature. This is the rainy season. Inversely, the northernmost ITCZ displacement and the equatorial front result in the presence of cooler and dryer air masses, which come from the southwest from upwelling regions. This is the dry season (Rossel and Cadier, 2009).

4.3 Tropical Mesoscale Convective Systems

A Mesoscale Convective System (MCS) is an organized group of thunderstorms that produces a contiguous precipitation area measuring about 100 km or more in at least one direction. This system grows upscale from convective towers to a convective-stratiform coupled vertical circulation, ultimately meeting its demise as only a stratiform rain region. Tropical convection is most often organized into mesoscale systems, with length scales of 100-1000 km and duration of several hours.

MCSs produce as much as 90% of rainfall in certain land areas. For the global tropics, they produce more than 50% of the rainfall in heavily raining areas (where the average annual rainfall is greater than 3 mm/day).

In the northwestern coast of South America, the Pacific-side of Colombia and Ecuador, MCCs are commonly found within April (Fig. 2) in timing with the southern displacement of the ITZC and the maxima of off shore moisture over the Pacific. On the other hand, MCCs in January (Fig. 1) are not commonly seen in the Equator; instead, MCCs are located on the south of the continent. Fig. 1 illustrates locations over the Ecuadorian and Pacific coast where the highest concentrations of MCCs often occur. This MCCs climatology includes all types of MCSs that match the 85 GHz Ice Scattering criteria defined in Mohr and Zipser (1996).

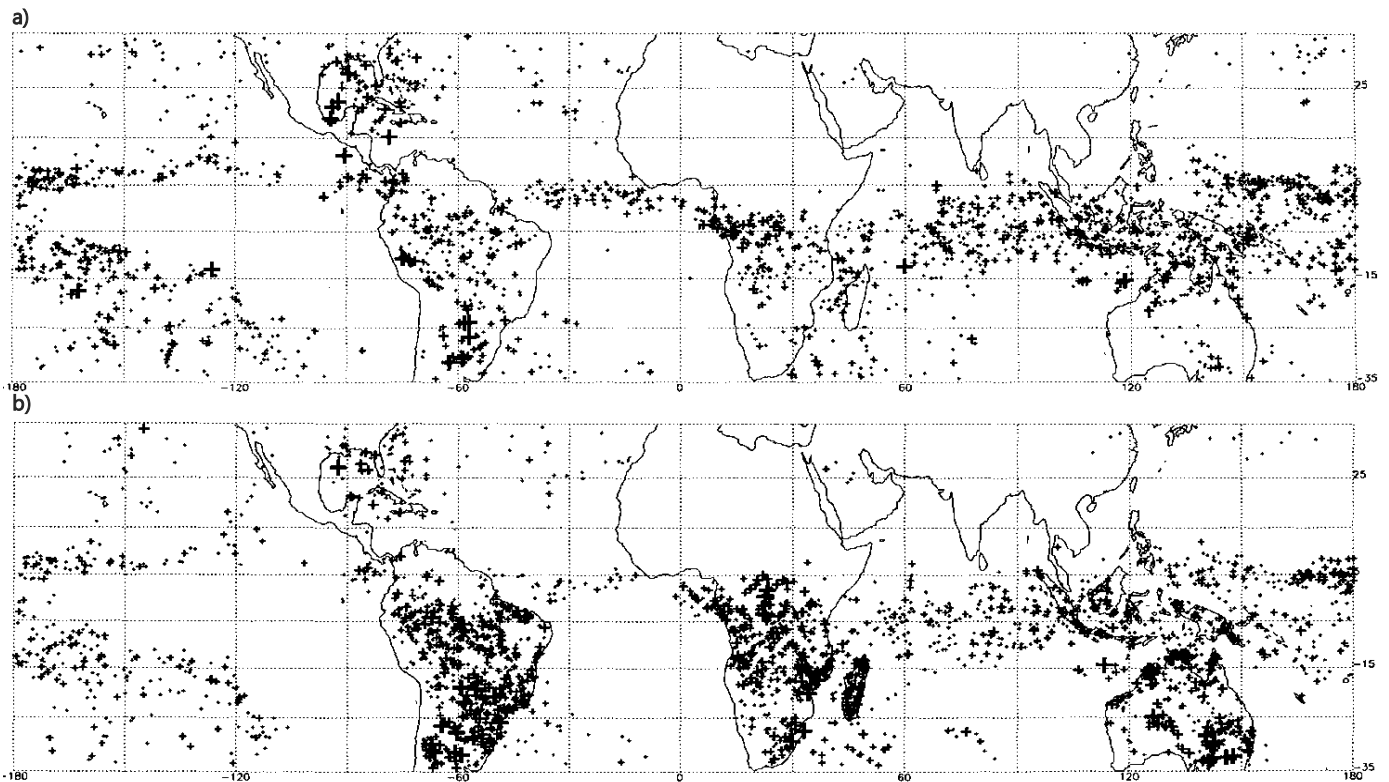


Figure 1. Climatology of Mesoscale Convective Systems in January measured by a Special Sensor Microwave/Imager (SSM/I) 85 GHz Minimum Polarization Corrected Temperature. a) sunrise passes b) sunset passes (Mohr and Zipser, 1986).

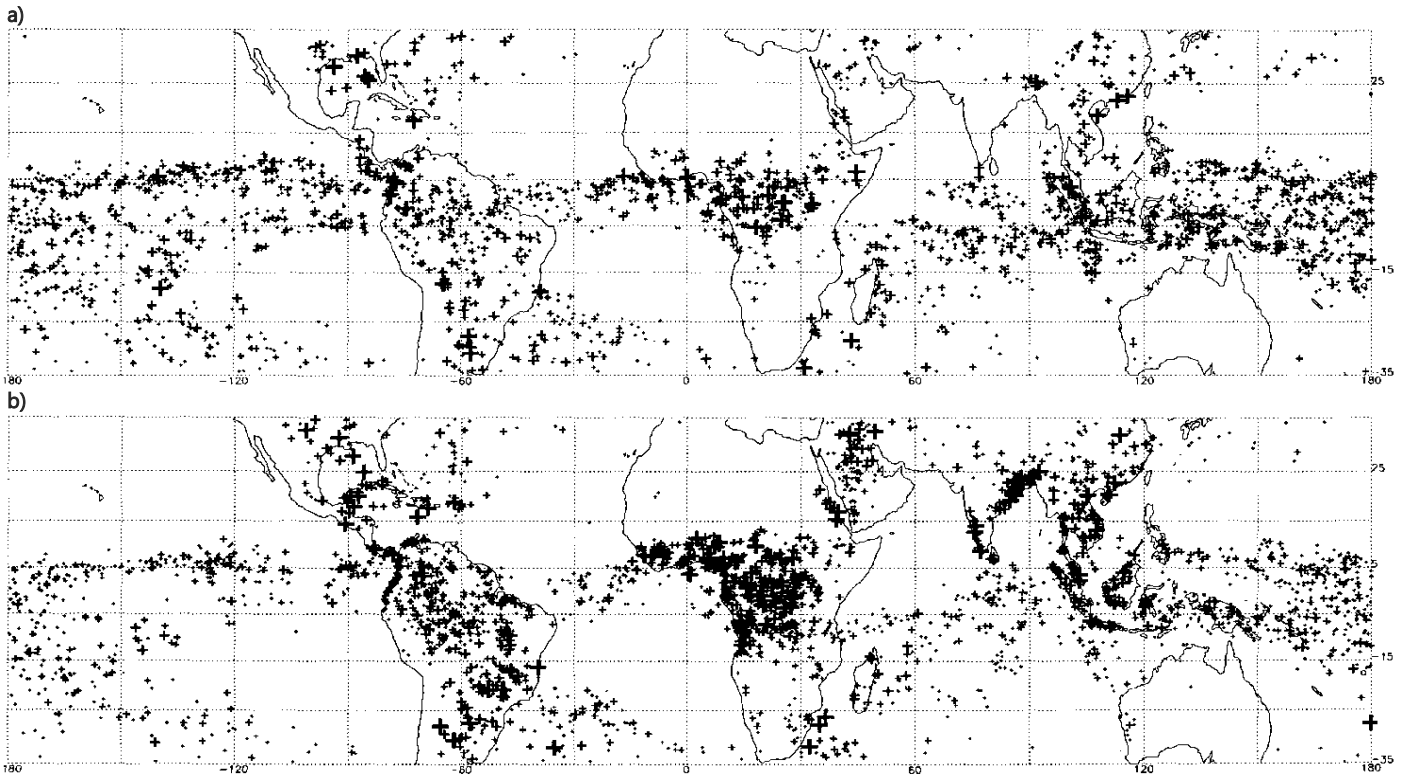


Figure 2. Climatology of Mesoscale Convective Systems in April measured by a Special Sensor Microwave/Imager (SSM/I) 85 GHz Minimum Polarization Corrected Temperature. a) sunrise passes b) sunset passes (Mohr and Zipser, 1986).

4.3.1 Structure

MCSs contain complex updraft and downdraft structures. However, most mature MCSs can be represented as mesoscale updrafts and downdrafts whose arrangement/tilt can differ between the types/modes. The tilt of the updraft is dependent on the environmental shear.

At certain times in their lifecycle, each MCS will precipitate from either or both a grouping of convective towers or a stratiform cloud deck. The organization of the stratiform and convective precipitation varies depending on the type/mode. Sometimes different modes occur as stages of a MCS lifecycle.

The most prominent dynamical features in MCSs are convective updrafts and downdrafts and a mesoscale updraft/downdraft coupled in the stratiform region. The updrafts originate from low-level convergence, which in turn builds convective towers through layer lifting/overturning (Fig. 3).

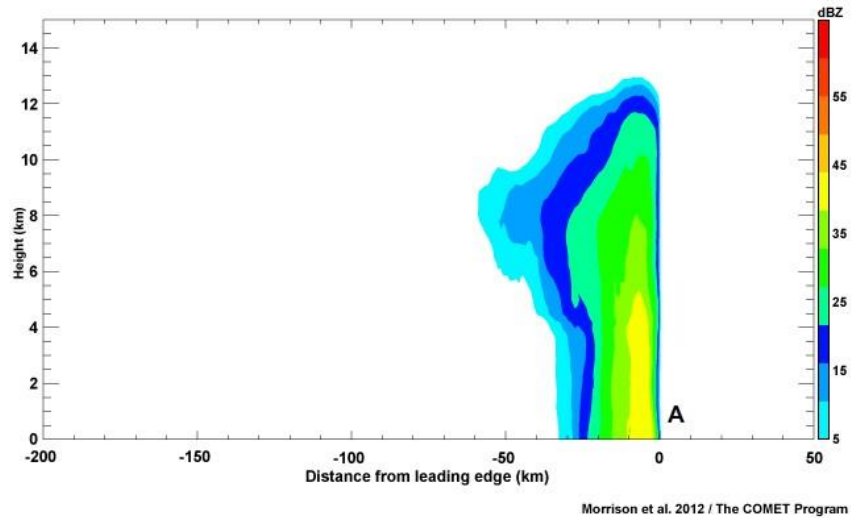


Figure 3. The dynamic structure of MCCs: Updrafts (Morrison et al., 2012).

Depending on the environmental shear profile and the system motion, these lofted particles will blow upstream, downstream, or both creating a broadening anvil on satellite imagery and increased low reflectivity in that direction over time. This creates the stratiform precipitation area (Fig. 4).

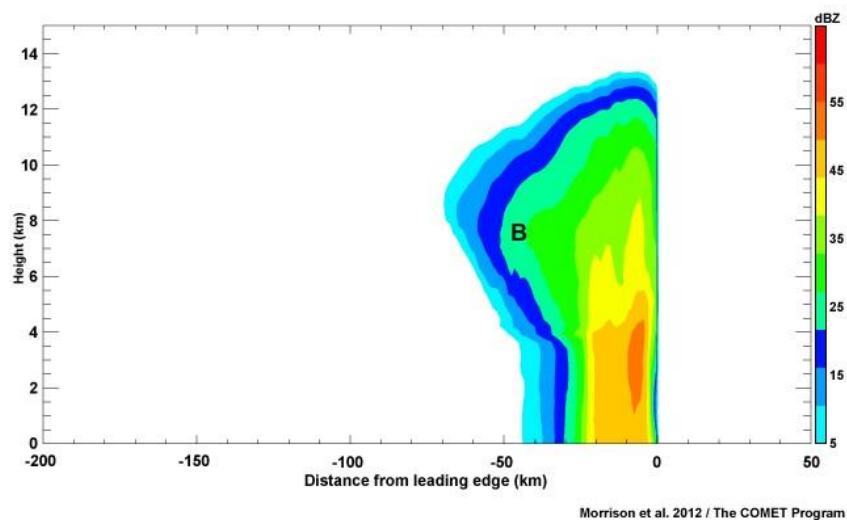


Figure 4. The dynamic structure of MCCs: Stratiform precipitation area (Morrison et al., 2012).

These lofted particles slowly fall out of the stratiform cloud. As the particles fall, latent cooling (from melting and sublimating particles at or around the melting level and at stratiform anvil cloud base) and precipitation loading make a downdraft and cold pool (Fig. 5). Some of this downdraft/cold pool air pushes toward the convective updraft at or near low levels increasing the low-level convergence, thus creating a positive feedback that enhances the updraft. The melting of ice particles in the stratiform region generates a layer of high reflectivity called the "brightband".

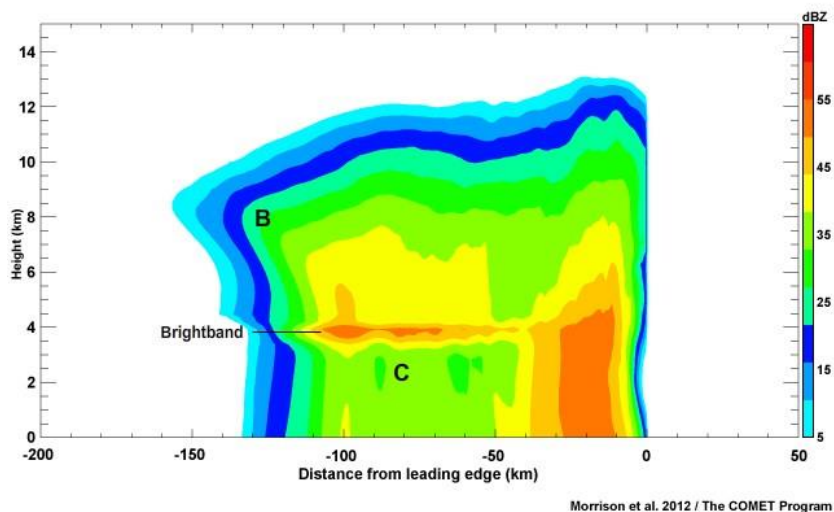
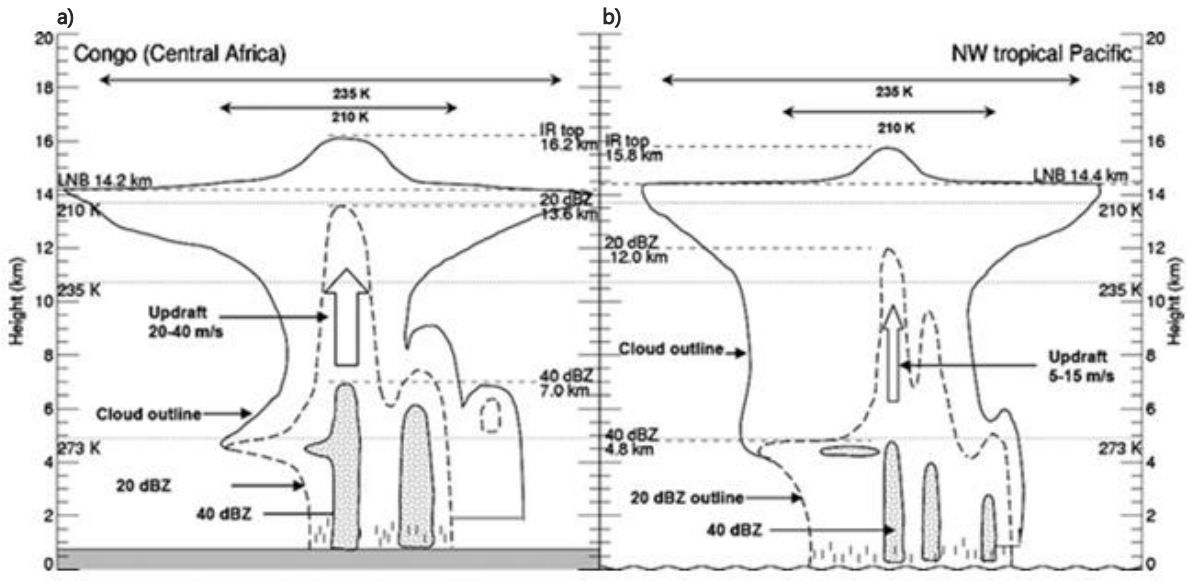


Figure 5. The dynamic structure of MCCs: Enhanced updraft due to feedback mechanisms (Morrison et al., 2012).

The strength and extent of the updrafts and downdrafts vary between continental and oceanic MCSs in the tropics. Typically, oceanic systems have weaker updrafts and thus shorter reflectivity cores and they are also larger than continental MCSs. Fig. 6 shows some of the differences between continental (left; Congo) and oceanic (right; NW tropical Pacific) mesoscale convective systems.



Liu et al. 2007

Figure 6. Schematic of the structure of deep convection over a) Central Africa and b) the northwestern tropical Pacific, demonstrating differences between typical strong systems in the two regions (Liu et al., 2007).

4.3.2 Types

Since MCCs are organized by their environmental wind shear, we can then explore different types/modes of MCSs from least to greatest environmental shear. The most common types of MCCs are:

4.2.2.1 Non-squall Tropical Clusters

The Non-squall tropical clusters is one of the types of the Tropical Mesoscale Convective System that has a low environmental shear before its beginning, and never reaches a strong shear between 700 and 250 hPa. The non-squall clusters are completely different to the squall cluster/line, which exhibit a strong mid-level jet in the 700-600 hPa layer that means an ample shear. Due to the lack of shear in the mid-levels, non-squall tropical clusters will align with the shear vector and, for this reason, almost none gains energy because of the generation across the shear vector (UCAR/COMET, 1997).

4.3.2.2 Mesoscale Convective Complexes

Mesoscale Convective Complexes (MCCs) are big and long-lasting, characterized by their size and almost circular appearance on infrared satellite imagery. However, the precipitation pattern under the cloud top could be similar to the squall line structure. MCCs usually reach the peak of precipitation intensity between 03:00 am with a duration around 6 to 12 hours. In addition, MCCs have greater environmental shear in the low-levels than non-squall tropical clusters. MCCs, however, do not show much shear in the low-levels as the case of squall line/bow echo systems (UCAR/COMET, 1997).

4.3.2.3 Squall Clusters/Lines

Squall lines or squall clusters are edges of thunderstorms forming along or ahead of a cold front. Their duration is also around 6 to 12 hours and their time span is long enough to be influenced by the Coriolis force effect, depending on the latitude. Most of the cases start with a set of convective towers that begin from the same activation mechanism. Furthermore, squall lines usually move quickly and are less prone to produce tornadoes than supercells. Their area could be large, but are typically only 20 to 40 km wide.

4.3.2.3.1 Bow Echoes

Bow echoes are a special case of the squall line that has a convex or bow-shaped leading convective line. They form where strong rear-to-front mid-level flow, called a rear-inflow jet (RIJ), goes down to the surface close to the head of the squall line. The bow echoes often cause their collapse relatively rapidly (1-3 hours) caused by the cutoff of the ascending movement that generates the layer-lifting and convective towers (UCAR/COMET, 1997).

4.3.2.4 Mesoscale convective Vortices

Sometimes the MCS (tropical or mid-latitude) is large or has an extended duration; it can develop its own mid-level mesoscale circulation caused by the Coriolis effect and thermal processes. Mesoscale Convective Vortices (MCVs) form in the stratiform region of MCSs. MCV is formed by the stretching of vorticity due to the mid-level latent heating in the stratiform region. The heating produces a warm anomaly that activates a dynamic response: expanding isentropic layers, a positive potential vorticity anomaly, and a mesoscale convective vortex. Some studies/observations demonstrate that the generation of subtropical MCVs tends to occur more often at lower latitudes than in mid-latitude MCVs (UCAR/COMET, 1997).

4.4 Esmeraldas river basin

The Esmeraldas river is formed by the join of many tributaries such as Blanco, Canandé, Guayllabamba, Toachi and Quinindé rivers. The watershed has an extension of around 21418 Km². The headwaters of this basin are located in the Ecuadorian Andean Mountains, on the slopes of glaciers Cayambe, Antisana, Sincholagua, Cotopaxi, Illiniza, Atacazo and Pichincha volcanoes (Fig. 7). In Ecuador, the highest precipitation volumes occur in the Amazon region and in the northwest of the Esmeraldas province, thus the Esmeraldas river basin drains one of the most water rich regions. The influence of the air masses that come from the Pacific Ocean separates perfectly two different rain periods: the rainy season, which goes from January to May, and the summer/dry season - that is notorious in the southern part of the basin as compared with the north that is rainy throughout the year. The annual precipitation total overpasses 3000 mm and the monthly values are usually above the 200 mm and, sometimes, it achieves 500 mm. In addition, the trade winds from the amazon basin cause precipitations almost during all the year on the upper basin, but the December-January period has less quantity of rain. This amazon influence is more sensible in the eastern and upper part of the basin (Pourrut, 1995; Cruz et al., 1977).

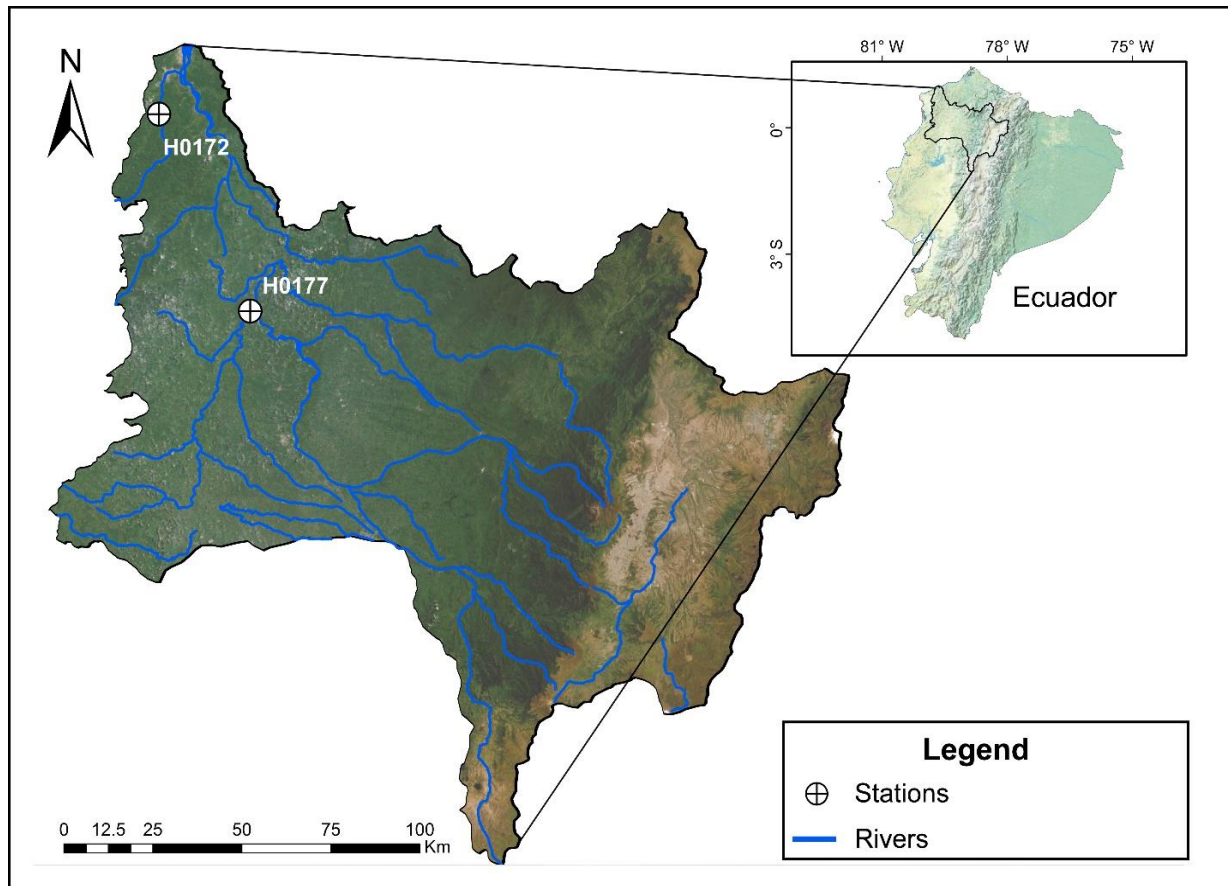


Figure 7. Study area showing INAMHI hydrological stations (white circles) and the main rivers in the Esmeraldas basin (blue lines). H0172 (Teaone) and H0177 (Quinindé)

4.5 The January 2016 flood

In the last decade, the relationship between regional climate and extreme rainfall events in the northern part of the Ecuador has not been concordant with those patterns observed during the first decade of the 21st century (Bendix et al., 2011; Pineda and Willems, 2018). Some years the climatic extremes did not result in heavy rainfall and floods, while others massive flooding brought destruction and disruption of socio-economic activities. That is the case of the January 2016 flood in Esmeraldas where an extreme rainfall event happened that led to serious floods in the region. Many of the rivers increased their water flow. The stations in Esmeraldas recorded 244.5mm in 24 hours, and westward, the Muisne station recorded 88.5mm. The event started to increase at 23:00 on 24th January during all the evening and early morning of the 25th of January causing floods.

Additionally, many rivers of the region overflowed. This is the case of the Teano River in Esmeraldas and Atacames, in Quinindé the rivers Blanco and Quinindé, and the Santiago river in Eloy Alfaro (Fig. 8b).

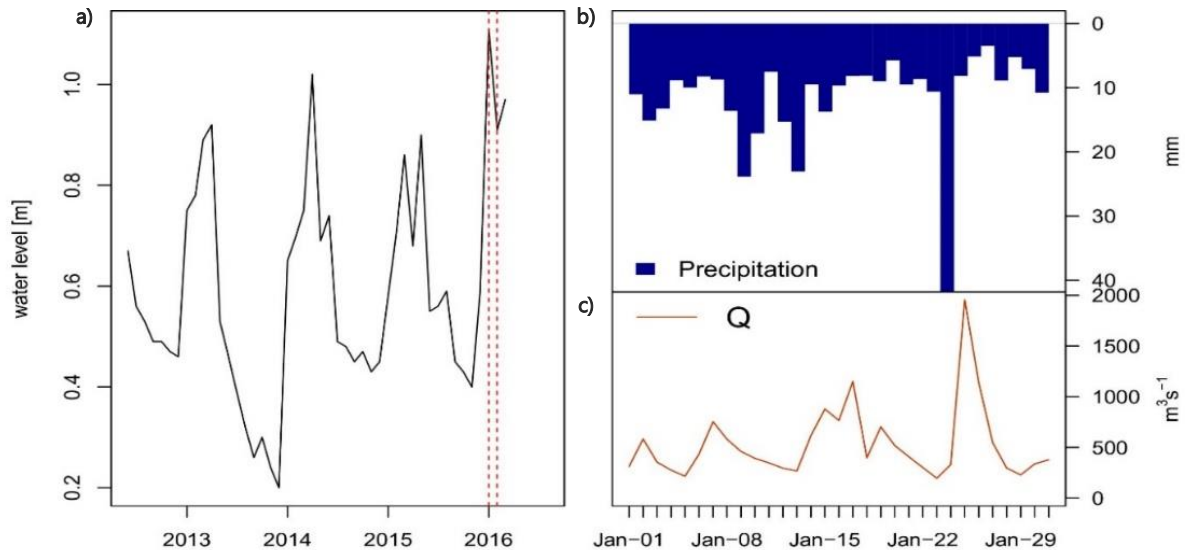


Figure 8. a) Water level in station Teano (H0172). Broken-line window shows January 2016. b) Average catchment station precipitation upstream station (H0177). c) River discharge in station Quinindé (H0177) in January 2016.

Specifically, Teano River showed in its limnometric gauge station an anomalous behavior for water level in January 2016 as compared with past years, at that month the water level in the river recorded more than 1.0 m. In addition, this event showed high discharge values in Quinindé River (Fig. 8a). During the first part of January, the discharge values did not surpass 1000 m³/s, in contrast, during the event the stream gauge recorded values around 2000 m³/s. Furthermore, the same pattern happened for the average catchment station precipitation in Quinindé river basin, at the beginning of the month the mean average showed low values (10 mm-20 mm) while in the event the precipitation peak overpassed 40 (mm) (Fig. 8c).

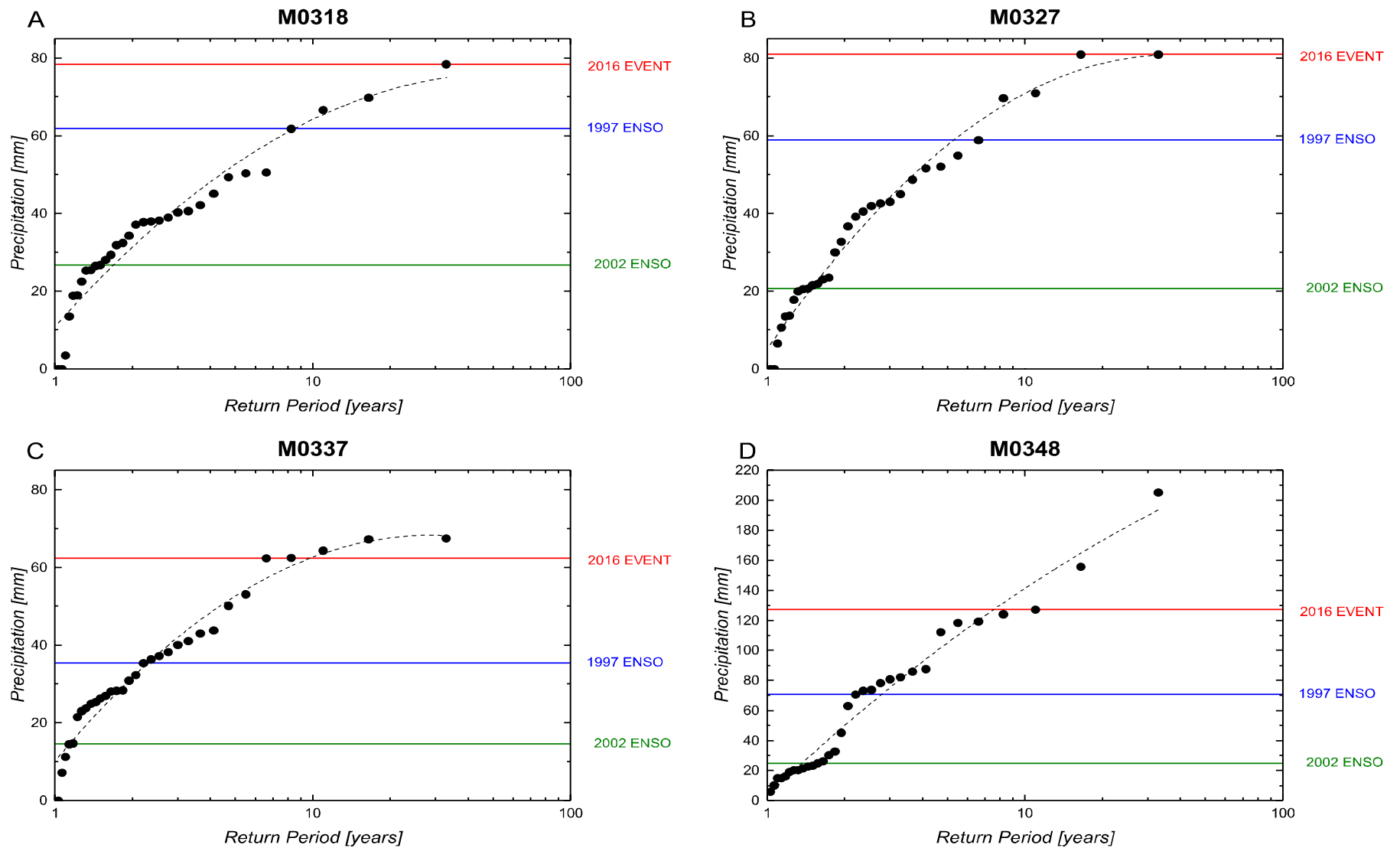


Figure 9. Empirical return period (years) vs monthly maxima precipitation (mm) in January for the 1987-2018 period in selected meteorological stations. (Dots) with trend line (dashed-line). Horizontal lines show the January 2016 event (red) and the 2002 and 1997 ENSO events. a) Apuela-Intag (M0318), b) Chontal Bajo (M0327), c) San José de Minas (M0337) and d) Santa Anita (M0348).

Furthermore, the return period analysis is a useful tool that represents the time in which a flood, earthquake, or other geophysical phenomena might occur again. Fig. 9 shows the empirical return period for the monthly maxima of precipitation in January for representative stations: M0318, M0327, M0337 and M0348 located in the basin within the 1987-2018 period, together with 3 extreme events: the January 2016 event, and the 1997, 2002 ENSO events. The graph reveals the severity of the January 2016 event over the northeastern (stations M318 and M327) in which this event shows the largest return period in the record. On the other hand, station M337 on the northeastern deep valley shows some extreme events with a magnitude slightly larger than the January 2016 HPE while on the southern part of the basin, station M0348 that records about 120 mm during the HPE, there are some extreme events that considerably overpass the magnitude of the January 2016 HPE. In all cases, the January 2016 extreme event exceeds the heavy rainfall recorded during ENSO years.

5. MATERIALS AND METHODS

This study focuses on the climatological reconstruction of the January 2016 flood event in Esmeraldas by using satellite and gauge data analysis. This information is useful to reconstruct the atmospheric conditions leading to this catastrophic climatic event in coastal Ecuador. In order to achieve it, some different techniques were used as: hydrometeorological characterization, precipitation and river flow data, wind circulation, satellite imagery and spatial fields of precipitation.

5.1 Hydrometeorological characterization

Using rainfall data recorded at meteorological and climatological stations from the Instituto Nacional de Meteorología e Hidrología (INAMHI) and satellite imagery from the Geostationary Operational Environmental Satellite (GOES) it is possible to create an atlas of hietograms and contour maps describing daily rainfall characteristic during the high precipitation event. This information is useful to classify the storm type, size, and duration. Furthermore, spatial fields are generated using geostatistical interpolation techniques to investigate the spatial structure of the storm.

5.2 Precipitation and river flow data

From INAMHI we obtained different types of information related to the high precipitation event. INAMHI stations work under regulations proposed by the World Meteorological Organization (WMO) and they are also equipped to measure the following atmospheric variables: air temperature, atmospheric moisture, atmospheric precipitation, heliophany, evaporation, wind and cloudiness, among others. The meteorological stations take hourly measurements between 07:00 and 19:00 hours, in the main climatological and ordinary stations the observation frequency is twice and three times a day respectively. In the case of pluviometric stations, three, two and one observations are taken at different times (7:00, 13:00 and 19:00). All the information is then processed in order to provide a homogeneous statistical sample on a national scale (Table 1).

Table 1. Meteorological stations with daily precipitation data for the period 1985-2018 divided by sub-basins.

<i>Code</i>	<i>Name</i>	<i>Coordinate UTM WGS1984 17S</i>		<i>masl</i>
		<i>x</i>	<i>y</i>	
<i>Output Rio Esmeraldas Basin</i>				
M0441	SAGUE(SAN MATEO)	652015	10097696	15
M0444	TEAONE-TABIAZO	646299	10087897	100
<i>Rio Blanco Basin</i>				
M1190	SAN BERNABE	712767	9998404	600
M1186	COOP. U. GANADEROS ORENSES	723716	9991614	760
M1185	MAR DE LA TRANQUILIDAD	733520	9976774	840
M0116	CHIRIBOGA	746635	9976342	1750
M1192	EL PASO	741932	9971519	2200
M0354	SAN JUAN- PICHINCHA(CHILLOG.)	763277	9968135	3440
<i>Rio Guayllabamba Basin</i>				
M1191	MONTE OLIVO - HCPP	726715	10020739	650
M0327	CHONTAL BAJO(GUAYLL.DJ ALAMBI)	750285	10025874	675
M1184	LA DELICIA-HCPP	726375	10015762	1480
M0339	NANEGALITO	758392	10007008	1580
M0362	LAS PAMPAS	726246	9952566	1583
M0318	APUELA-INTAG	776517	10038908	1620
M0326	SELVA ALEGRE-IMBABURA	769465	10026891	1800
M0325	GARCIA MORENO	763866	10025599	1950

M0009	LA VICTORIA INERHI	811395	9992993	2262
M1156	NAYON GRANJA SANTA ANA - PUCE	786112	9980055	2284
M0337	SAN JOSE DE MINAS	789949	10018320	2440
M0346	YARUQUI INAMHI	798614	9981959	2600
M0343	EL QUINCHE-PICHINCHA	799945	9988321	2605
M0345	CALDERON	786856	9988753	2645
M0361	NONO	769931	9991520	2710
M0909	GUALSAQUI	788244	10035131	2710
M0113	UYUMBICHO	775216	9956670	2740
M0024	QUITO INAMHI-INNAQUITO	779893	9981193	2789
M0358	CALACALI INAMHI	776646	9999786	2810
M0359	CAYAMBE	818204	10005597	2840
M0363	SIGCHOS	734555	9922270	2880
M0353	RUMIPAMBA-PICHINCHA	787405	9952333	2940
M0023	OLMEDO-PICHINCHA	828417	10016019	3120
M0344	CANGAHUA	815109	9993300	3140
M0335	LA CHORRERA	774138	9977322	3165
M1183	RUNDOPAMBA	773273	9989645	3320
M1231	ILLINIZA-BIGROSES	760264	9930739	3461
M0364	LORETO PEDREGAL	786223	9937519	3620
M0357	CANAL 10 TV.	775531	9981409	3780
<i>Rio Quinindé Basin</i>				
M0160	EL CARMEN	674820	9970915	260
M0348	SANTA ANITA-KM.10 VIA CHONE	694704	9974138	560

5.3 Wind circulation:

5.3.1 National Centers for Environmental Prediction (NCEP) and the National Center for Atmospheric Research (NCAR) Reanalysis

The NCEP/NCAR reanalysis 1 is a product developed by National Oceanic and Atmospheric Administration (NOAA), this project (denoted “reanalysis”) to produce a 40-year record of global analyses of atmospheric fields in support of the needs of the research and climate monitoring communities. This effort involves the recovery of land surface, ship, rawinsonde, pibal, aircraft, satellite, and other data; quality controlling and assimilating these data with a data assimilation system that is kept unchanged over the reanalysis period 1957–96. This eliminates perceived climate jumps associated with changes in the data assimilation system. NCEP/NCAR reanalysis

lis a system useful to perform analysis/forecast using past data from 1948 onwards. The data storage has two different temporal coverage, 4-times daily/daily and monthly values for 1948/01/01 to present and long term monthly means, derived from data for years 1981 – 2010. A vast group of this data is available from the Physical Sciences Division in its original 4 times daily format and as daily averages. Nonetheless, the information for the period 1948-1957 have some differences in the regular gridded data (non-Gaussian). These data were performed at 8 times daily in the model, due to the available inputs at that time it was accessible at 3Z, 9Z, 15Z, and 21Z, while the 4 times daily information were available at 0Z, 6Z, 12Z, and 18Z. The combined result of this early era is 8x daily using the last forecasted times (Kalnay et al., 1996). With this powerful data, it is possible to generate large-scale circulation composites, choosing for this case study the specific humidity and horizontal winds at 850 hPa in order to represent the lower circulation.

5.4 Satellite imagery:

5.4.1 Geostationary Operational Environmental Satellites

Geostationary Operational Environmental Satellites (GOES) is able to detect electromagnetic radiation that allows us to know the presence of clouds, water vapor and surface characteristics. This system works in a different way than the terrestrial radar systems, in the case of terrestrial systems; they use the return signals of the energy waves that are released to the atmosphere. In contrast, the GOES work by passively sensing the energy.

The satellite system works with the reflected sunlight (visible) and thermal energy (infrared) that came from the surface of the earth, clouds and atmosphere. One principal difference with terrestrial stations is that visible images are only available during daylight hours when sunlight reflects. However, the information emitted by the earth is continuous (24 hours) and these satellites are able to read all this continuously huge data.

GOES-13 imagers have one visible channel with a center wavelength of 0.65 μm (channel 1), and four infrared channels consisting of a shortwave infrared window channel with its wavelength centered at 3.9 μm (channel 2), an infrared water vapor channel located at 6.5 μm (channel 3), a longwave infrared window channel centered at 10.7 μm (channel 4), and a longwave infrared carbon dioxide channel whose wavelength is located at 13.3 μm (channel 6). The spatial resolution (i.e., instantaneous geometric field of view) of the visible channel is 1 km and that of the infrared channels is 4 km at the subsatellite point, except for GOES-13 channel 6. Additionally, the five

GOES channels are designed for different purposes. At the wavelength of channel 4 (10.7 μm), most surfaces and cloud types have an emissivity close to 1 and the energies emitted by the earth's surface or cloud are not significantly attenuated by the atmospheric gases. Therefore, brightness temperatures at channel 4 measured by the GOES satellite are close to actual surface skin or cloud-top temperatures except for thin cirrus. In contrast to channel 4, channel 6 is located within a region of the earth's emitted spectrum (13.3 μm) where a considerable amount of both cloud- and surface-emitted radiation is attenuated by carbon dioxide molecules. (Zou, Qin & Zheng, 2015).

Satellite images were retrieved from the Comprehensive Large Array-Data Stewardship System (CLASS) that is a useful on-line tool for the distribution of NOAA, US Department of Defense (DoD), Polar-orbiting Operational Environmental Satellite (POES) data, NOAA's GOES data, and derived data. From this library, we can obtain the images from GOES 13 over the study region during the time of the event.

Table 2. Detailed information of satellite imagery retrieved from CLASS system.

<i>Satellite imagery details</i>	
Product	Goes-13
Acquisition date	25-01-2016
Band	4
Name Band	Longwave infrared window
Wavelength	10.7 μm
Objective	Surface or cloud-top temperature, precipitation, etc.

The Integrated Data Viewer (IDV) is a free software developed by the University Corporation for Atmospheric Research (UCAR) for 3D geo-visualization. It is a very useful tool to view and analyze a vast set of geo-information in a compact and integrated manner. Some of the capacities of this software is the processing of satellite images, gridded data (numerical information came from prediction models), surface observations (METAR), upper air surveys, National Weather Service (NWS) NEXRAD Level II, RADAR Level III data and GIS data, all this in just one unified interface. Additionally, IDV allows a friendly and easily interchange of information with different common scientific data servers and other users (Unidata, 2019).

The satellite images retrieved from the CLASS were processed in the IDV software. For this case of study, the Infrared (IR) channel from GOES-13 allows us to obtain a 2D image from a selected area. Afterwards, the planar image was processed in ArcGIS software for an easier manipulation.

5.4.2 Climate Hazards group Infrared Precipitation with Stations

Climate Hazards group Infrared Precipitation with Stations (CHIRPS) data set was developed in order to provide a smart interpolation technique and high-resolution estimations and long-term precipitation records based on infrared Cold Cloud Duration (CCD) measurements. Its algorithm is based in a 0.05° climatology that join satellite information to reproduce precipitation on non-gauged locations. In addition, it presents 0.05° CCD-based precipitation estimates daily, weekly and monthly. Correlates station data with the satellite information to present a pre-product with a latency of 2 days and a final product with a latency of about 3 weeks. Finally, it presents a current combination technique that integrates the spatial correlation structure of the CCD-estimates to assign interpolation weights. CHIRPS algorithm, it is very useful for monitoring extremes events, help us quantifying the hydrologic impacts of decreasing precipitation, rising air temperatures, support effective hydrologic forecasts and trend analyses, etc. (Funk et al., 2015). For this case study, CHIRPS data was used to generate spatial fields of precipitation in order to investigate the spatial structure of the precipitation associated with the mesoscale convective complex.

5.4.3 Tropical Rainfall Mission Measurement 3B42

Tropical Rainfall Mission Measurement (TRMM) 3B42 was used to monitor the sub-daily evolution of the storm. TRMM 3B42 and other Sensors provide precipitation estimates in the TRMM regions that have the (nearly-zero) bias of the “TRMM Combined Instrument” precipitation estimate and the dense sampling of high-quality microwave data with fill-in using microwave-calibrated infrared estimates. The granule size is 3 hours. The precipitation estimates are available at 0.25° grid intervals of latitude from 50° N to 50° S and 0.25° grid intervals of longitude from 180° W to 180° E (Huffman et al., 2007).

5.5 Spatial fields of precipitation:

There are several techniques available in the literature to derive spatial fields based on gauge information as well as to merge/fusion point-based information with gridded data. In the Andean region, there is not general agreement on which technique suits a particular application since their performance to interpolate gauge data over complex terrain depends on the density and the spatial heterogeneity of ground observations. In this case study spatial precipitation fields are derived by i) interpolating only point-based information, and ii) merging ground data with satellite products. Then the technique/product that best fits ground observations was selected. For this, the following geostatistical and non-parametric methods were used (Nerini et al., 2015):

5.5.1 Mean Bias Correction

Mean Bias Correction (MBC) is a way to correct the satellite information by the use of the total multiplicative bias between the rain gauge estimates and the collocated satellite values, thus assuming a uniform bias over the spatial domain (Nerini et al., 2015). The correction factor B , for each daily event, is calculated by:

$$B = \frac{\sum_{j=1}^N Z_G(x_j)}{\sum_{j=1}^N Z_S(x_j)} \quad (1)$$

Where:

N = number of available gauges inside the satellite domain.

$Z_G(x_j)$ & $Z_S(x_j)$ = the gauge and satellite daily rainfall values corresponding to gauged location j .

5.5.2 Double-Kernel Smoothing

Li and Shao (2010) proposed the Double-Kernel smoothing (DS) technique especially for data-sparse purposes. This method uses the residual points ε_S using the kernel density function and the correction of the satellite information by the estimate of residual field. The residual point at the corrected location $j=1, \dots, N$ is defined to be

$$\varepsilon_{S_j} = \varepsilon_S(x_j) = Z_S(x_j) - Z_G(x_j) \quad (2)$$

The first part of the interpolation generates a complete group of residuals (pseudoresiduals) ε_{SS} on the same grid as the data from satellite. At that gridpoint location $i = 1, \dots, M$ the pseudoresidual is defined to be:

$$\varepsilon_{SS_i} = \frac{\sum_{j=1}^N \Lambda(\|H_i - H_j\|/b) \varepsilon_{S_j}}{\sum_{j=1}^N \Lambda(\|H_i - H_j\|/b)} \quad (3)$$

Where $\|\cdot\|$ represents the Euclidean norm and Λ is the Kernel function defined as a Gaussian kernel following Li and Shao (2010):

$$\Lambda(\|H_i - H_j\|/b) = \frac{1}{\sqrt{2\pi}} \exp\left[-\frac{1}{2}(\|H_i - H_j\|/b)^2\right] \quad (4)$$

H is the position of the points, and b is the bandwidth determined using Silverman's rule of thumb (Silverman, 1998)

$$b = \left(\frac{4\sigma^5}{3n}\right)^{1/5} \quad (5)$$

Where n is the amount of samples and σ is the standard deviation of the samples. The second part of the interpolation is applied in the residuals and pseudoresiduals in order to calculate the final error field ε_{DS} :

$$\varepsilon_{DS_k} = \frac{\sum_{j=1}^N \Lambda(\|H_k - H_j\|/b_1) \varepsilon_{S_j} + \sum_{i=1}^M \Lambda(\|H_k - H_i\|/b_2) \varepsilon_{SS_i}}{\sum_{j=1}^N \Lambda(\|H_k - H_j\|/b_1) + \sum_{i=1}^M \Lambda(\|H_k - H_i\|/b_2)} \quad (6)$$

Finally, the merged product z_{DS} at point k is calculated by subtracting to the satellite estimate z_{S_k} the corresponding error ε_{DS_k} :

$$z_{DS_k} = z_{S_k} - \varepsilon_{DS_k} \quad (7)$$

The DS interpolation of the residuals values does not follow the stationary assumption, different to geostatistical methods (Nerini et al., 2015).

05.5.3 Ordinary Kriging

Ordinary kriging (OK) was first introduced by Matheron (1969) which is a case of kriging with changing mean where the trend is modelled as a function of coordinates. Other authors also agree that the term ordinary kriging should be reserved for the case where only the coordinates are used (Hengl, 2003). Mathematically OK is expressed by:

$$\hat{Z}(S_o) = \sum_{i=1}^N \lambda_i Z(S_i) \quad (8)$$

Where:

$Z(S_i)$ = the average value in the location i

λ_i = an unknown weighting for the value measured at location i

S_o = location of the prediction

N = the amount of measured values

5.5.4 Kriging with External Drift

In the case of Kriging with external drifting (KED) instead of using monomials of the coordinates such as in the OK equations, the drift is defined externally through some auxiliary variables such as parameters derived from digital elevation modelling, remote sensing imagery, and thematic maps. This is probably the most preferred name used for kriging with auxiliary information (Hengl, 2003). Mathematically KED is expressed by:

$$\hat{Z}_{KED}(S_o) = \sum_{i=1}^N \omega_i^{KED} \lambda_i Z(S_i) \quad (9)$$

Where:

$Z(S_i)$ = the average value in the location i

λ_i = an unknown weighting for the value measured at location i

S_o = location of the prediction

N = the amount of measured values

ω_i^{KED} = auxiliary value weight from KED

6. RESULTS AND DISCUSSION

6.1 Storm properties

The satellite images for the event of January 2016 over the Esmeraldas river basin were retrieved directly from the CLASS system developed by NOAA in a poorly processed data format. Afterwards, the software IDV was used to determine some characteristics of the study event such as duration, area, etc.

6.1.1 Life span

The storm of January 2016 in Esmeraldas started in the early morning of the 25th lasting around 16 hours until late in the afternoon. The heavy rains with the largest cloud sizes in the storm occurred from 09:00 until 15:00 (Table 3). Those values are consistent with storm features previously observed in mesoscale convective events near Piura region (Peru), during around 6 hours of heavy rains and 16 fully developed storms (Goldberg et al., 1987).

Table 3. Cloud area measured by satellite imagery using longwave IR window (band 4) from GOES 13.

<i>Time</i>	Area (km²)	
	< -32°C	< -52 °C
2:15	18554	14337
4:15	53061	36116
6:15	95633	51846
8:45	138985	70680
10:15	173468	88273
12:45	178116	87573
13:15	175302	72525
16:15	112080	22299

6.1.2 Area

A MCC is a part of the MCS. This MCC could be identified from MCS using IR information retrieved from GOES satellite imagery. Many authors have commonly agreed with the parameters that these phenomena show. Starting by a cloud shield with repeatedly low IR temperatures colder than -32°C with a coverage area up to 100000 km^2 . Consequently, the inner part presents a cold cloudy region colder than -52°C with a coverage area up to 50000 km^2 . Additionally, these complexes regularly have a duration around 6 to 12 hours and produce heavy amounts of rain, thick hail, harsh winds and tornadoes in the first phase of the MCC progression (Maddox, 1980).

The size of the storm cloud retrieved from satellite imagery methods is useful to determine the characteristics of the studied event. Fig. 10 shows the development of the storm during the complete day (25th January 2016) since around 02:00 to 17:00, showing the size of the center of the cloud and the peripheries over the Esmeraldas basin. The red colors represents the part of the cloud with the lowest temperatures less than 52°C (Center cloud). In the studied case, the internal cloud shows an area that rounds the 14337 Km^2 for the small size to 88273 Km^2 the biggest one. The green/yellow colors represent the peripheries of the cloud with temperatures less than 32°C . For the Esmeraldas storm, the part of clouds with these features has extended areas compared with the central parts. The areas with these temperatures range from 18554 Km^2 in the early morning to 178116 Km^2 at noon (Table 2). The area covered by the storm in its peak of rain it covers the complete Esmeraldas basin, moreover, most of the northwestern part of the country was also affected by the event.

In addition, the cycle of the storm seen in Fig.11 shows that onset occur in the northern part of the Esmeraldas river basin at the beginning of the storm, then it covers the complete upper part of the basin. After that, clouds cover the complete basin during the morning. At noon, the storm start to dissipate in a westward direction towards the Ecuadorian coastal region. Anyway, the heavy rains of the storm are concentrated most of the time in the central part of the basin.

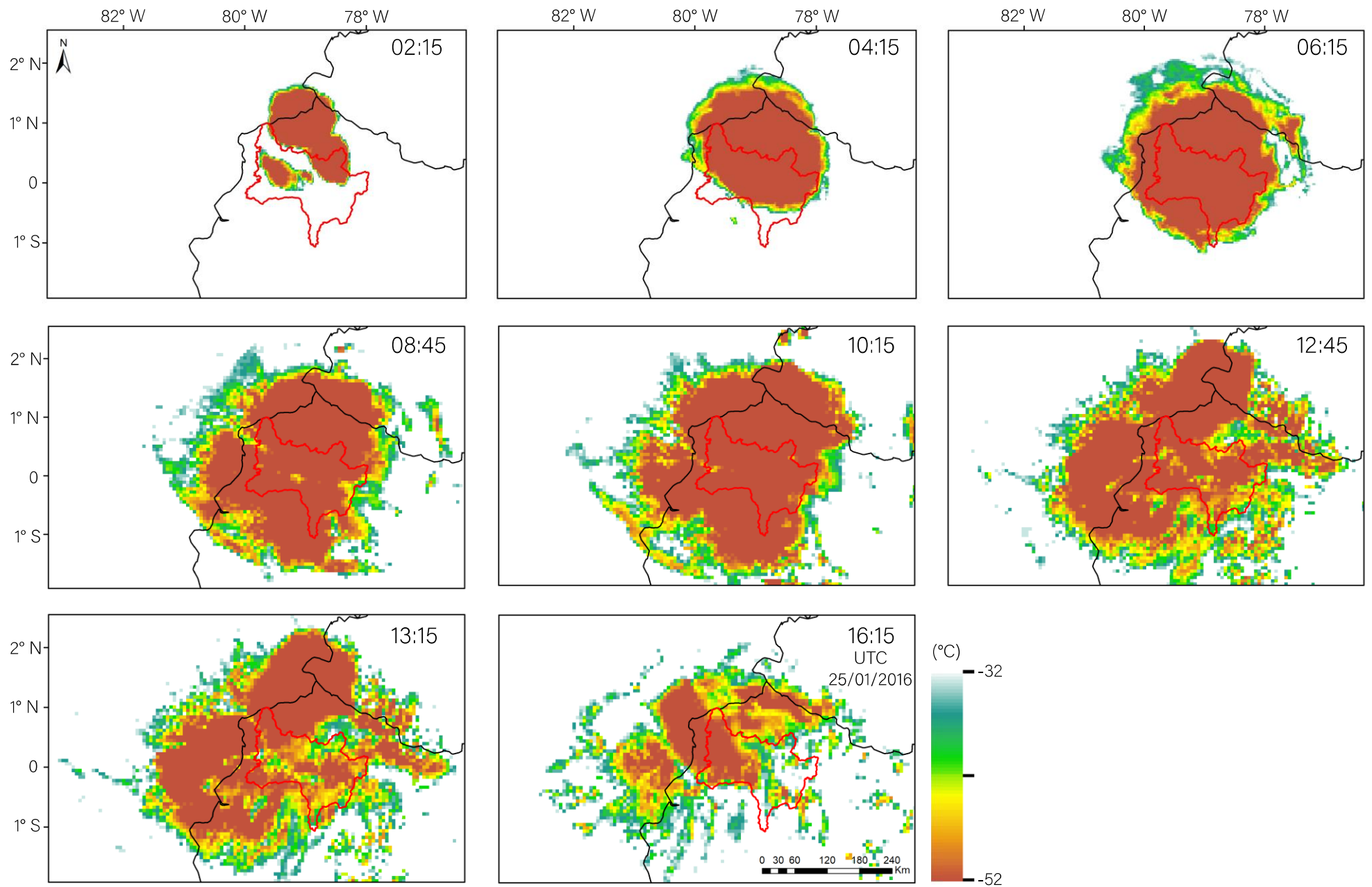


Figure 10. Development of the storm cloud during the event day (25/01/2016) as observed via satellite GOES 13.

6.2 Precipitation

Fig. 11 shows the precipitation measurements in mm recorded by the INAMHI stations along the Esmeraldas river basin during the day of the storm and two days before. The values of the 25th for rain are high in comparison with the values for the 24th and 26th. The peak value is 176.50 mm in the central part of the basin and the low values (0 – 10 mm) are located in the eastern part of the basin. It is remarkable that the concentration of the heavy rains in the INAMHI stations network is in the central part (Andes-coast transition region) and not in the coastal part of the basin. Anyway, there are not many stations in the eastern part of the basin to make a complete comparison. Nevertheless, the precipitation values of the 25th allow us to clearly determine that it is a separated event compared to the preceding days (Fig.11).

In addition, hietograms from precipitation values also give us information about patterns in the different stations along the Esmeraldas basin. The stations located in the outlet of the basin M0444 and M0442 show different behaviors each one. In the case of low altitude stations, the values are low and show a small peak in the event day. On the other hand, the high altitude station presents different pulses of precipitation during the month.

The next group of stations belongs to the Rio Blanco basin where precipitation values are fairly constant throughout January. Except, for station M1192 which is located in the central part of the Rio Blanco sub-basin. Here, the values for the event day have a considerable peak reaching 100 mm of rain.

For the case of the Rio Guayllabamba northern sub-basin, it is clearly visible one particular feature in most of the stations; the values through the month are low in comparison with the event day. Most of the values of the other days are comparatively lower than those for 25th January except for the highest station of this sub-basin, the station M0358 that is located in the central part of this sub-basin at 2810 masl.

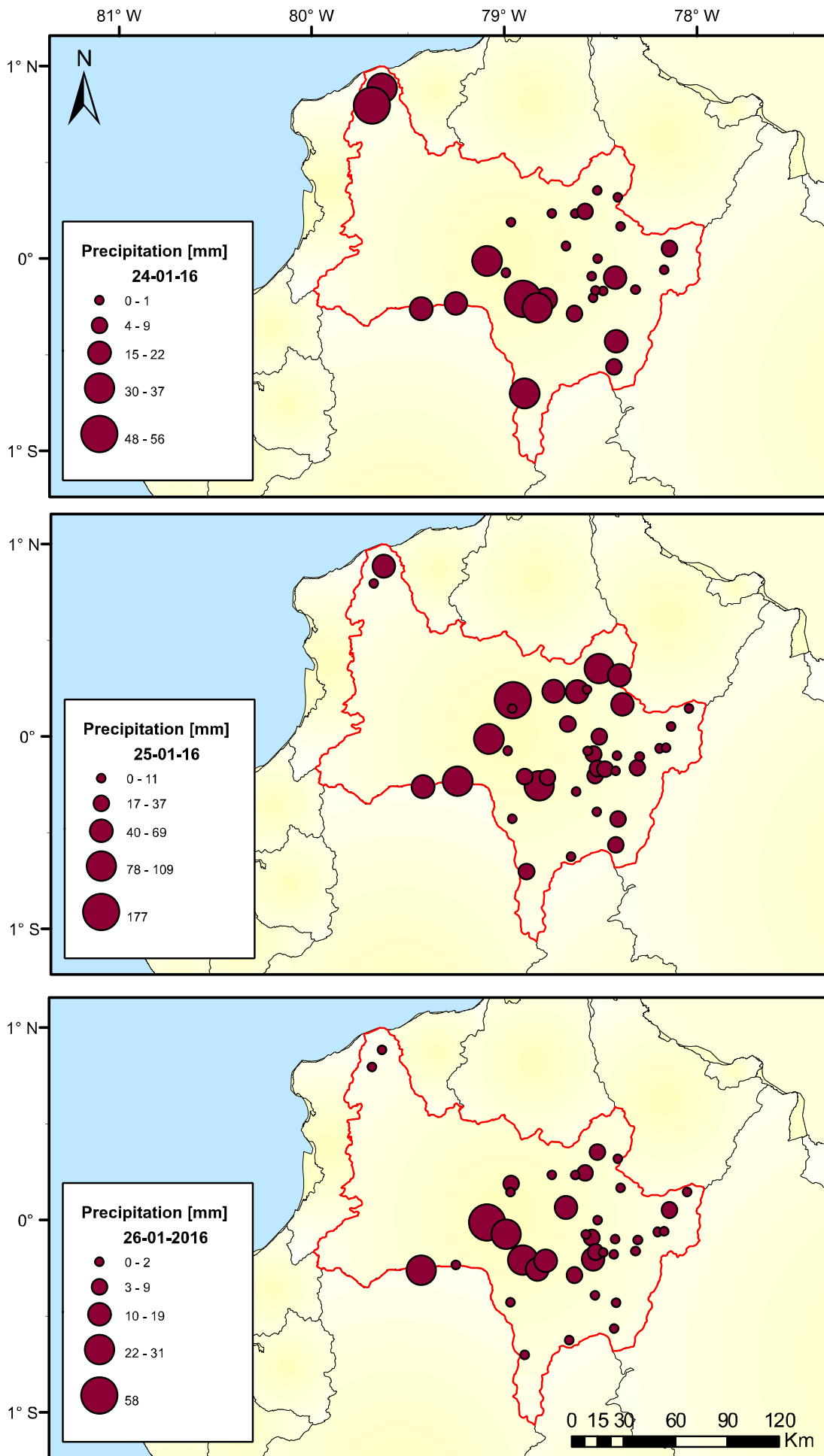
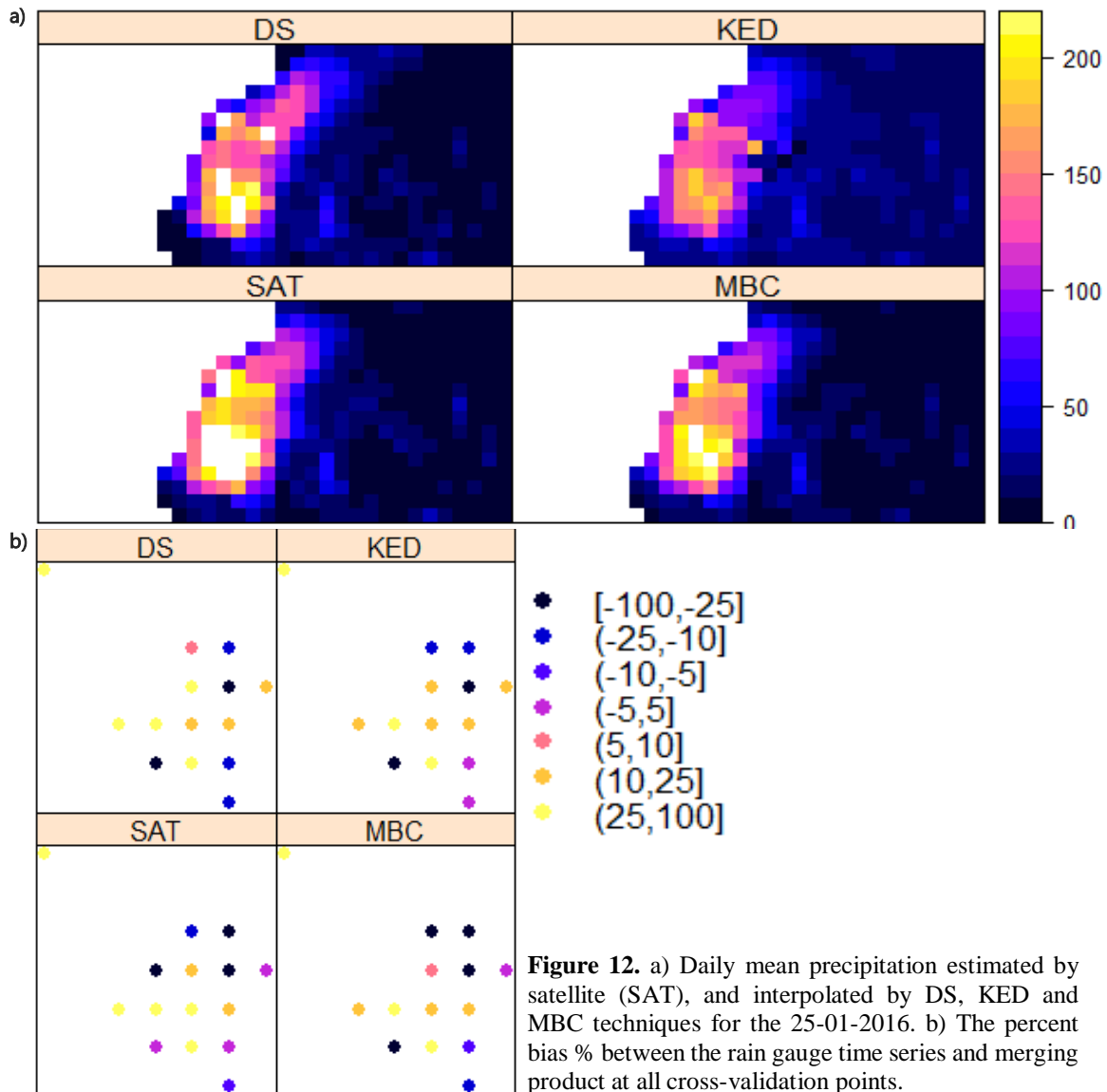


Figure 11. Daily precipitation (mm) retrieved from INAMHI stations during a) 24th, c) 25th and c) 26th of January 2016

In addition, in this group of stations, the highest value for the event day is found, that is 176.5 mm. Finally, in the Rio Guayllabamba southeast basin, many stations have different pulses of rain during the entire month. However, it is also clear that they have a peak or anomalous behavior in the 25th event in all of this sub-basin stations. On the other hand, in station M0359 the event it is not very clear, this behavior is possible due to its peripheral location inside of the Rio Esmeraldas basin.

The interpolation techniques used for the analysis in this study were the DS, KED and MBC. Fig.12a shows the different interpolation techniques compared with the precipitation values retrieved from satellite imagery. In addition, an estimation of percent bias is presented for each technique in order to know which method works better for this specific case (Fig.12b).



KED technique has a low percentage of bias, meaning that this interpolation technique has a better degree of confidence. Furthermore, the interpolation graph of the KED and satellite imagery (SAT) data shows similar patterns and values of precipitation. From the blended gauge-satellite grid, it can be concluded that the high precipitation associated with the MCC extended far south from the Esmeraldas basin affecting also the neighboring Guayas river basin.

6.3 Climatological Analysis

To address the question whether the January 2016 HPE can be regarded as an extreme weather event ascribed to the December-February climatology or to any other large-scale climatic forcing, the December-February climatology was investigated in terms of weather states following the approach by Pineda & Willems, 2016. That is a weather pattern decomposition based on machine learning techniques, specifically, a Hidden Markov Model (HMM) (Hughes and Guttorp, 1994) that breaks the December-February climatology into 4 weather states. Composite anomalies of NCEP-NCAR reanalyzes of specific humidity synchronized with horizontal wind fields at 850 hPa for the four different states described by Pineda & Willems, 2016 were made available from former research. Those atmospheric composites were computed as anomalies of the December-February climatology.

It is important to describe the main climatological patterns during the December-May season as foreground for the atmospheric composite interpretation of the sub-season ones. During the December-February sub-season, the ITCZ migrates to its southernmost location point close to the equator in the eastern Pacific driven by strong northeastern trade winds over the Central American isthmus, and the southern retreat of the South Pacific anticyclone which results into weak southern trade winds. On the other hand, during June–August the South Pacific trade winds become stronger because the southeastern Pacific anticyclone is at its northernmost position, then the ITCZ stays north of the equator (Pineda & Willems, 2016).

The analysis of the December-February sub-season in terms of the four weather states provides a picture of the long-term climate setting which can be interpreted as the expected climatological conditions during this sub-season. First, the state 1 (658 days), the wettest state, shows an excess of humidity in the eastern Pacific, offshore of Ecuador that extended to the central part of the country (Andean mountains) (Fig. 13a). The winds converge around the Equator. They appear as

both winds that came from the south with a northeast direction and winds from the north with a southwest direction. The state 2 (512 days), less wet than the first one, shows small gradients of specific humidity between 0 - 0.0004 and winds coming from the east with a northwest direction, thus it can be considered as a sub-state or a remainder of state 1 at high elevation (Fig. 13b). State 3 (985 days), the driest one, presents the lowest values in specific humidity, being the coldest state. The wind directions are not so clear, however, it shows some circulation patterns with a northwest direction (Fig. 13c). Finally, the state 4 (694 days) presents considerable amounts of moisture in the basin. The wind circulation shows the same pattern than state 3 with a southwest direction (Fig. 13d).

Figure 14a shows the daily sequence of weather states as output of the HMM. Specifically the output of the Viterbi algorithm (Viterbi, 1967), which decodes relevant features about the intra-seasonal and inter-annual variability in order to yield information about the climatology of the December-January sub-season during a 46-year period. Accordingly, the first weeks of December the dry state (state 3) prevails over the other states, although in some years the state 4 is also present.

On the other hand, in January the pattern change and the wet states 1, 2 and 4 dominate during most of the sub-season. The last weeks of January show occurrence of all states, meaning that average conditions for 25th January 2016 HPE, during the past 46 years, do not show a marked climatological pattern. Additionally, it is remarkable that during the El Niño phenomenon years (1983-1997) the wet states 1 and 2 are persistent through the sub-season. Fig 14b presents the four different states during December-January for each day during 46 years, for the first half of December is clear that the state 3 dominates over other states. The second half of the this month is controlled by the state number 4, and then the state 1, the wettest one, leads the occurrence of rainfall at the end of December through the entire January.

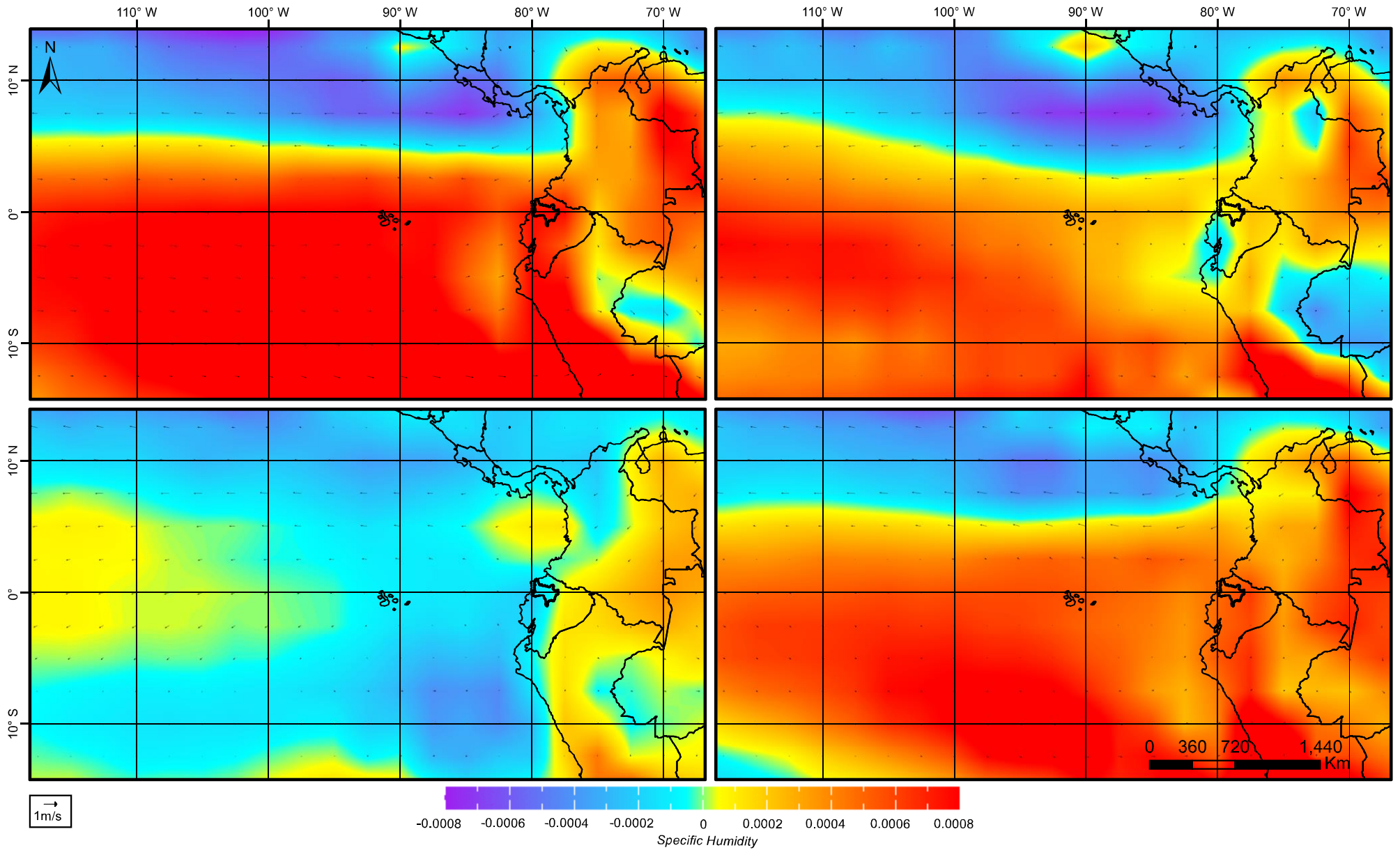


Figure 13. HMM state anomaly composites of horizontal winds (vectors) and specific humidity at 850 hPa (colors) with respect to December- February climatology for 1964-2010 (a)-(d) state 1-4 respectively.

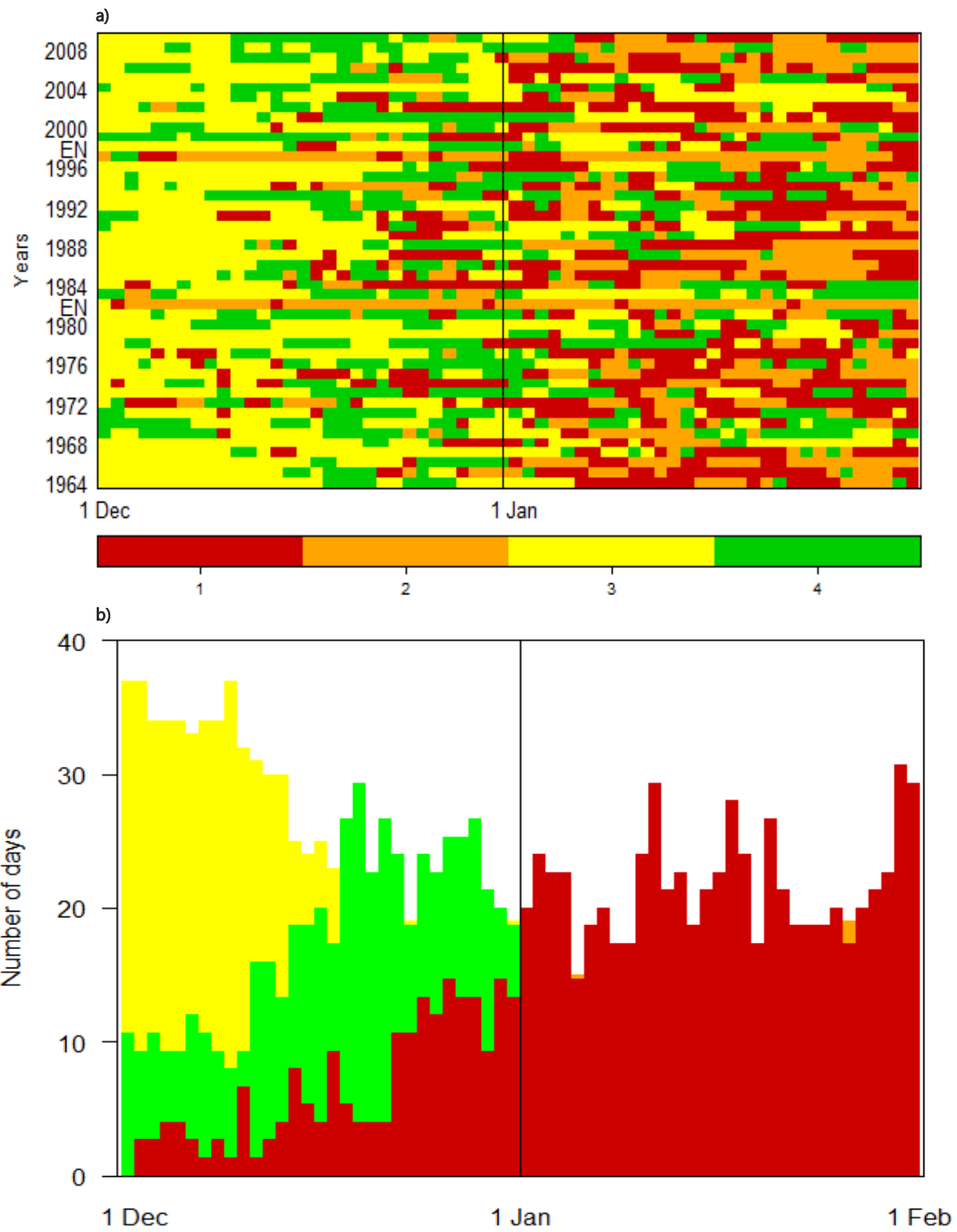


Figure 14. a) Viterbi sequence of most likely states 1964-2010 b) Climatology for each day during 46 years period. Colors represents states 1-4

In order to determine if the study event belongs to the regular January climatology of the past years, horizontal winds and specific humidity at 850 hPa were plotted for a period of 5 days before and after the event day (20th-30th January 2016). Fig.15 shows low-level specific humidity over the ocean region that help us to identify that this was not an event in which the Pacific atmospheric moisture was active. Furthermore, the highest values of atmospheric humidity are located along the Andean cordillera, but such moisture setting is different to the pattern observed for all four states which altogether describe the 46-year December-February climatology.

Finally, the wind analysis lets us know the direction of the low level circulation, which in this case shows an overall pattern pointing west. Additionally, it is clear that low-level wind velocity in the high precipitation weather event is higher than the one observed in the 46-year climatology, the order of magnitude overpassing the climatological wind speed is equal to 10, which is a considerable amount. In summary, the climatological analysis for the event day shows a particular pattern which differs from the 4 states describing the long-term December-February climatology, meaning that the factors that led to the occurrence of the HPE do not correspond with the expected climatological patterns for January, and thus, other atmospheric drivers might be responsible for the onset and development of the HPE.

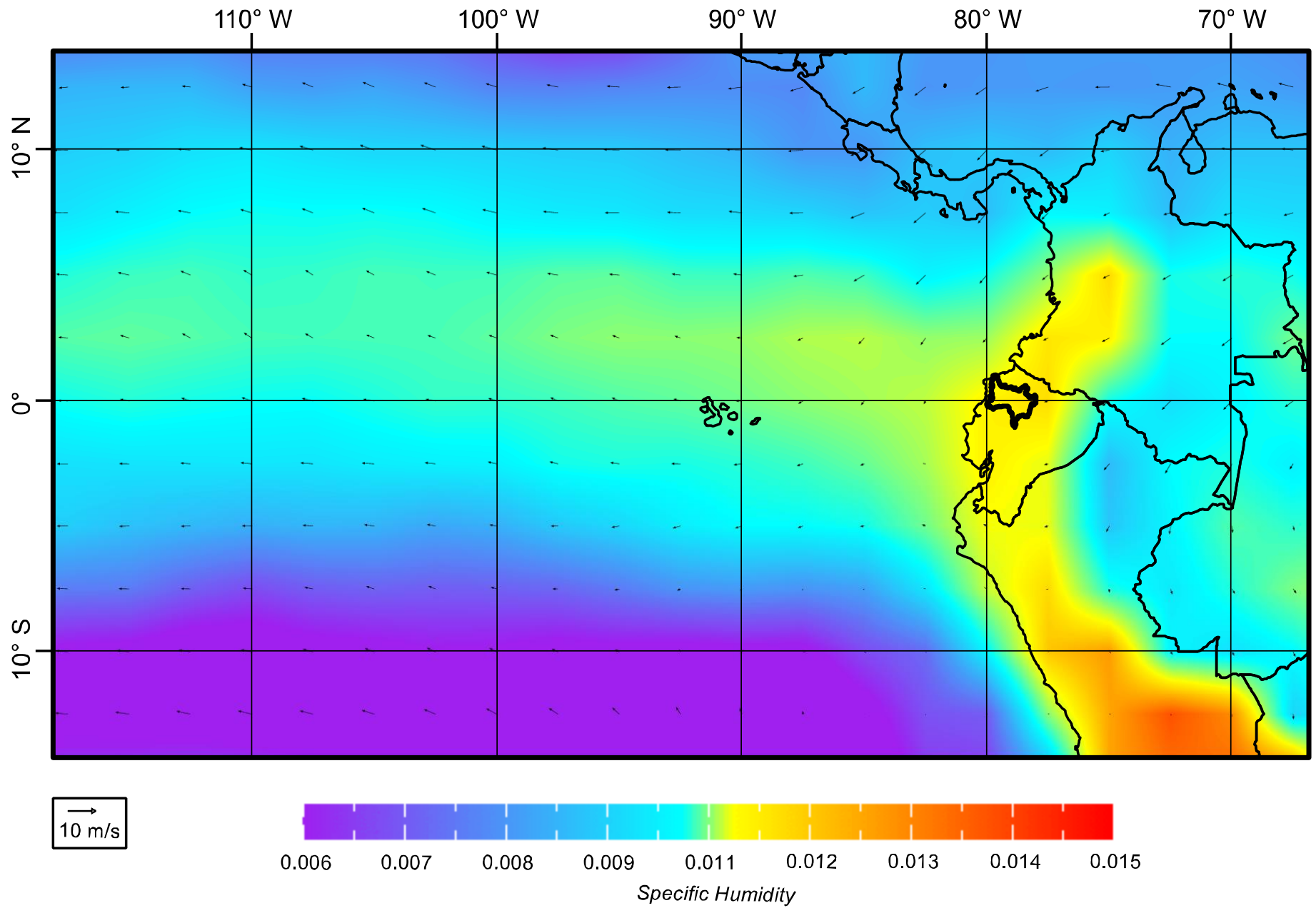


Figure 15. Climatological analysis for the period 20th – 30th January 2016 using horizontal winds (vectors) and specific humidity at 850 hPa (colors).

6.4 The January 2016 HPE

Many different features of the atmospheric circulation and landscape such as low-level moisture, wind circulation, orography, among others, determine the dynamics of an extreme weather event. In order to classify the type of storm that developed over the Esmeraldas basin in 25th January 2016 it is necessary to identify the meteorological parameters responsible for its genesis, propagation and dissipation.

The genesis of the HPE, as observed on GOES imagery (Fig. 11), begins with three isolated convective cells at around the 02:00, in which the biggest cloud covers an average area of 18554 km² (Table. 3). These three convective cells start to grow up in the north of the basin and expand to the south, being part of the very first updrafts and downdrafts of the MCCs formation (Fig. 3). The following hours the mature convective clouds are put together by easterly wind interactions to reach an area of around 53061 km² at 04:15. At this stage, the upstream of the convective cloud creates a broadening anvil that it is possible to recognize on the satellite imagery (Fig. 4). Following the cycle of the HPE, the cloud size increases with time, in which the brightband of the cloud melted ice particles in the stratiform region, reaching very large areas between 95633 km² and 112080 km². This stage of the MCC is caused by enhanced updrafts due to feedback mechanisms (Fig. 5). Additionally, the size of these clouds with large areas allows us to infer that the structure of the HPE is a typical tropical inland MCC, similar to those observed in Central Africa and described by Liu et al. 2007. For the wind shear field we can see in Fig. 15 that at low-level circulation with a propagation of 10 m/s causes a moderate wind shear at that level. As the MCC is fully developed, the winds move away from the unstable air, the convective pattern disappears and the precipitation slowly dies out.

One particular characteristic of the Esmeraldas basin is its terrain structure, this help to explain the particular pattern of precipitation in the north and southern part of the basin. Fig. 16 shows the topography of the basin, together with extreme precipitation values in the 25th January HPE. The basin's elevation range varies considerably due to the presence of high elevation ranges in the east part and low terrain in the west. The north-easternmost cordillera origins in the Cayambe volcano at 5790 masl and the Fuya Fuya mountain at 4290 masl; southward we have the Guayllabamba depression with an elevation of around 1800 masl The Ilalo volcano continues to form the eastern

cordillera with an elevation of 3161 masl, followed by the southern peaks of the Illiniza North 5248 masl and Cotopaxi volcano 5897 masl. The eastern mountain range described before has an average elevation of approximately 4000 masl and constitutes the basin water divide. The mountain range acts as an elevation barrier to the air mass that ascends from low to high terrains, until it reaches an altitude where it expands and cools adiabatically; thus, the atmosphere cannot keep humidity, creating clouds and rain. The phenomena it is known as orographic lifting and occurs in many parts of the Andean cordillera. However, it is important to clarify that in the north of the basin, just down of the Fuya Fuya mountain, there is a depression that dissects the eastern mountain range block causing a breaking off in the cloud barrier. This can be seen in Fig. 9, where rainfall in the stations M0318, M0327 and M0337 located in the north part of the cordillera shows a similar pattern, contrasting with station M0348 that shows a different behavior in the south. Fig. 17 shows the sub-daily evolution of the 24th-25th January storm, the genesis of the MCC was likely above normal moisture confined on the north-eastern part of the basin (at 22:30) which provided with convective updrafts due to orographic lifting driven by the N-S mountain barrier. This results into the first nocturnal convective showers (at 01:30). Due to updraft and downdraft mechanisms the storm developed to a cluster of convective showers on the central part of the basin (at 4:30), which later migrated to the lower basin where the highest intensities were found on the shore (at 7.30).

Finally, the climatology of the HPE (Fig. 15) shows high specific humidity values along the mountain cordillera and low values in the Pacific Ocean, meaning that the event is most likely not associated with ocean moisture action. Additionally, this event is not concordant with a 46-year January climatology as proposed in Fig. 13 because the atmospheric patterns for the 4 different states are not related to those observed during to the HPE. Winds are stronger in the study event than in the 46-year January climatology, and the specific humidity shows different patterns with its high and low values placed in different zones. In summary, the principal characteristics of the HPE allowed us to determine that is a Mesoscale Convective Complex, that in its genesis was constituted by orographic lifting, that matured with moderate low-level shear and weak mid-upper level shear. The propagation winds have a magnitude around the 10 m/s and the dissipation, caused by the movement of the winds from the unstable air disappeared the convective patterns causing a slow dead (Table 3).

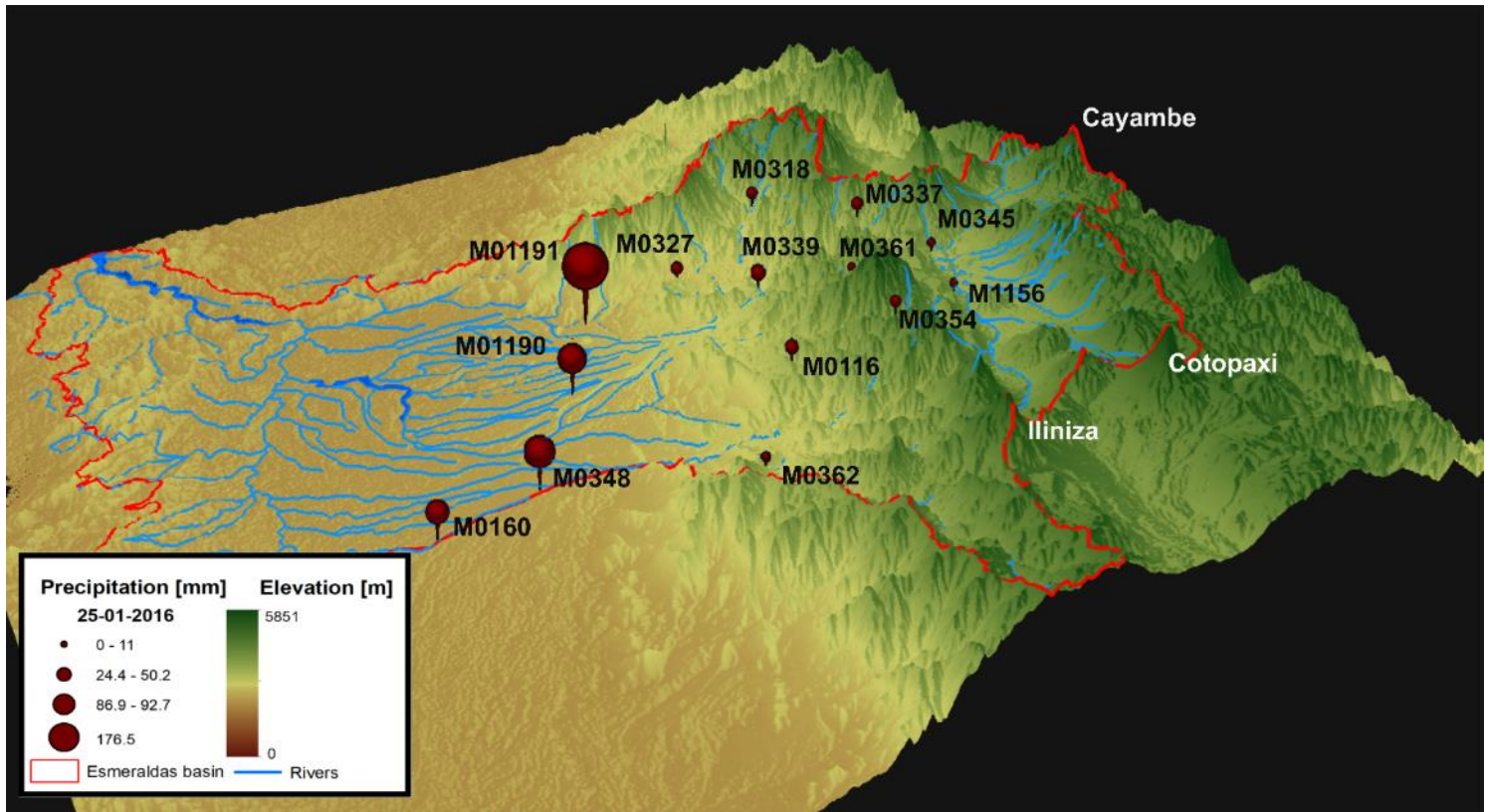


Figure 16. 3D terrain model based on Shuttle Radar Topography Mission (SRTM-dem) of Esmeraldas basin (red line) showing meteorological stations and precipitation on 25th of January 2016 (red-wine dots). The vertical scale is exaggerated 0.5x.

Table 4. Climatological characteristics of study event, genesis, wind shear, propagation and dissipation.

MCS Properties	
Type	<i>Mesoscale Convective Complex</i>
Genesis	Orographic lifting
Wind Shear	Moderate low-level shear, weak mid- to upper-level shear
Propagation	10 m/s
Dissipation	Winds moves away from the unstable air, the convective pattern disappears and the precipitation slowly die out.

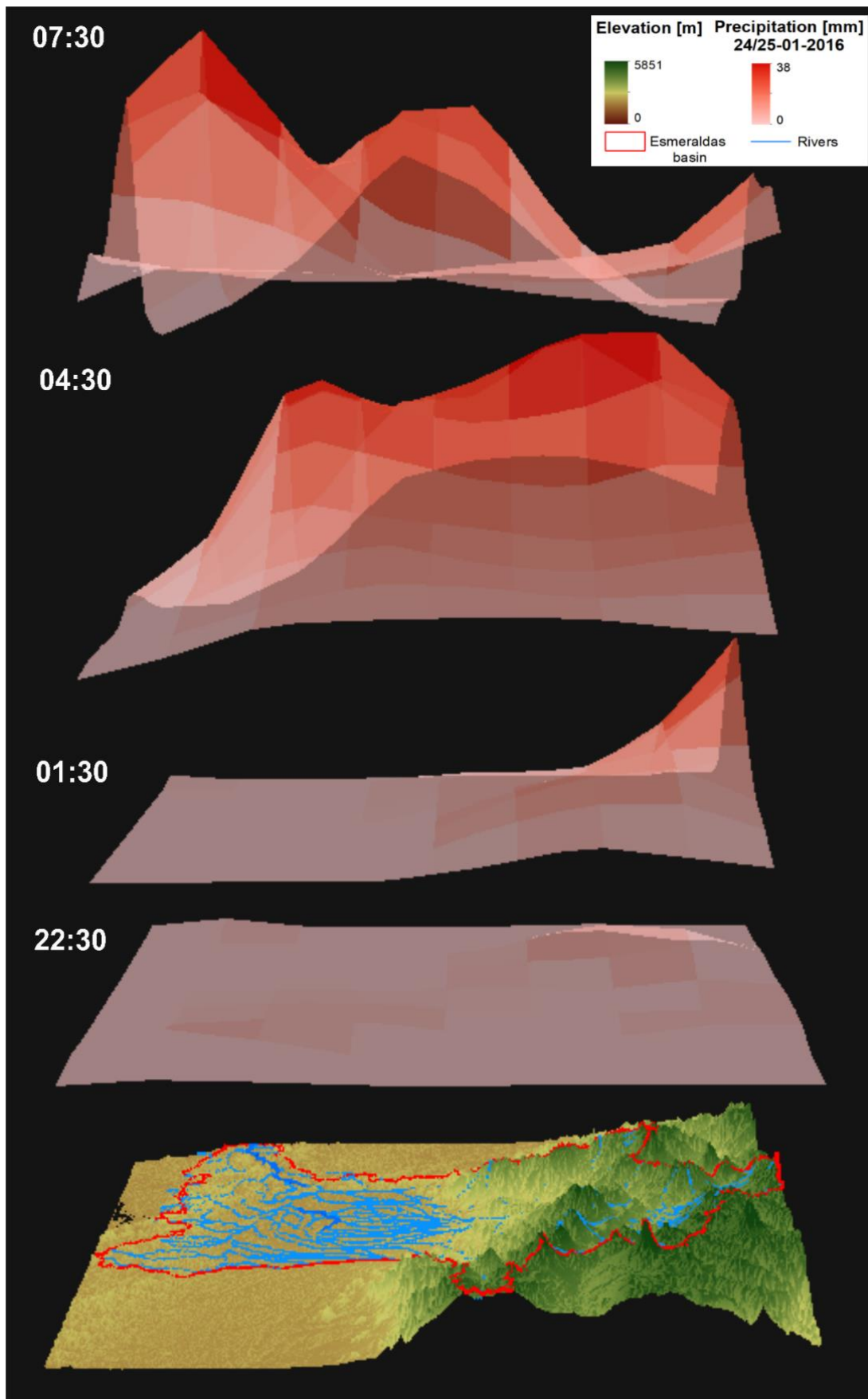


Figure 17. 3D terrain model of Esmeraldas river basin (red line) overlapped by TRMM precipitation data for 40 a time sequence of storm events recorded every 3 hours within 24th-25th January 2016. The sequence starts at 24th Januray at 22:30.

7. SUMMARY AND CONCLUSIONS

Because of the economic losses driven by heavy rains and floods in Ecuador and the lack of information about such extreme weather events in tropical meso-scale meteorological literature, this climatological reconstruction is essential to contribute to the knowledge of High Precipitation Event (HPE) dynamics. This latter is important for climate risk management, as it constitutes one stepping-stone towards building basis for the potential predictability of HPEs that lead to flooding in the region. This study has analyzed different sources of information about the heavy rainfall event that was precursor of devastating flooding in the Esmeraldas province in January 2016 and characterized it in a long-term climatological background.

Precipitation data retrieved from INAMHI ground station network shows that the highest precipitation values round 180 mm and occurred in 25th January; the days before and after the event show lower values implying that the HPE had a sub-daily life span. Additionally, the spatial distribution of the stations with high precipitation values is located over the central part of the Esmeraldas basin at a low to medium altitude range (0 – 1800 masl). This information allows us to infer that the core of the storm was located mainly in the north central part of the basin. This is concordant with the information retrieved from GOES 13 (satellite imagery) that shows the same spatial pattern.

In order to determine the type of storm, data retrieved from GOES 13 helped us to characterize the different features of the cloud top. The maximum area of the cloud at < -32 °C in its largest extent was around 178116 km² and at < -52 °C was around 88273 km² showing that the scale size of the rainfall system was meso- β (-25 to -250 km) (Goldberg et al., 1987). Regarding the duration of the storm, the event lasted 6 hours of heavy rains and around 16 hours of complete storm. Furthermore, the interpolation of the gauge data with satellite information by the KED technique allowed us to capture the spatial structure of the storm by merging information of the hydrometeor in the cloud top and precipitation recorded on ground. In this way, it was possible to track the storm genesis, development and its intensity over land, besides to infer cloud structure using information retrieved only from GOES 13. Furthermore, the KED interpolation output suggests

that in the south of the Esmeraldas basin there was also presence of heavy rains, which should be further analyzed.

Additionally, the 3D terrain model of the Esmeraldas basin shows a particular mountain cordillera that is located in the eastern part of the basin. This mountain range shows high peaks with an average altitudinal range of around 4000 masl for the cordillera, i.e. Cotopaxi volcano (5987 masl), Cayambe volcano (5790 masl), Illiniza North peak (5248 masl), Fuya Fuya (4290 masl), Ilalo (3161 masl). They all surround the Guayllabamba depression zone that reaches an altitude of about 1800 masl. This information allows us to determine that there is an eastern mountain range acting as a moisture and cloud barrier causing orographic lifting which helps the development of the updrafts and convection in the genesis of the HPE. Anyway, the northern part of the basin presents a small depression in the eastern mountain barriers that do not favor orographic lifting in that part, causing a different atmospheric moisture behavior in the zone. In summary, due to all the facts described above, it is possible to conclude that this heavy precipitation event belongs to the Mesoscale Convective Systems category, specifically a Mesoscale Convective Complex.

In addition, in order to investigate the relationship between the atmospheric conditions and the HPE, horizontal winds and specific humidity at 850 hPa (~ 1500 masl) data from the NCEP/NCAR reanalysis 1 product were analyzed. Four different states were chosen in order to characterize the climatology for 46-years of data. These states represent two wet states (state 1, state 2) followed by a dry state (state 3) and, finally, a quasi-wet state with some similar features to the state 1 (state 4). This technique showed that the predominant state in most of the 46-years climatology during the first half of December is the dry state (state 3), besides during the rest of the month and in January the pattern shifts to fluctuate between the wet states 1, 2 and 4. Additionally, the daily 46-year December-February climatology also shows that during the first days of December the state 3 dominates; the second part of the month is led by the state 4, and the final part of the December and the complete January is controlled by states 1 and 2.

In addition, by comparing the atmospheric conditions for the HPE, 5 days before and after the storm, with the 4 states retrieved from the 46-year climatology it is possible to conclude that this is most likely an isolated event. This is because the low-level atmospheric circulation shows different circulation patterns and strong winds in the HPE (10 m/s) which are different to wind velocities of about 1 m/s observed for the 4 states. In terms of moisture distribution, the HPE

atmospheric setting show a non-oceanic occurrence, which differs from the 46-year climatology of the proposed 4 states. It is particularly different to the wet states 1 and 2 characterized by air moist arising mostly from the Pacific Ocean and are active in January. Therefore, it is clear that this HPE does not belong to the usual January climatology.

In conclusion, the January 2016 heavy precipitation event over the Esmeraldas basin showed to have particular features that seem not to fit the December-February climatology. From a hydrological impact perspective, it might be regarded as an early onset of those heavy storms, often MCCs, that appear in the core of the rainy season (April) and whose driver is large-scale organized convection. Nevertheless, the evidence shown in this study suggests that such MCCs can also appear in January when both the surface processes and atmospheric circulation favor its genesis and development.

8. FURTHER RESEARCH

The future work in this topic should characterize more extreme rainfall events that some forecast models could detect with a useful lead-time in order to exploit the advantages of forecasting systems. Many other cases across the continent in the west and east of the Andes could help to better understand the dynamics of heavy rainfall formation and development in Ecuador; and the skills and limitations of forecast models to detect those weather anomalies. Furthermore, other methodologies could be applied to better understand the patterns of these types of storms and retrieve more characteristics of each event. In addition, it is necessary an improvement in the network of meteorological observations across the country to have better databases to support this type of studies.

The blending of ground data with satellite information showed that the core convective activity in the storm moved over the southern part of the basin following the moisture-cloud mountain divide. The study and tracking of these features will enable a better understanding on how the orographic lifting forces these kind of storms in this part of the cordillera. Finally, it is necessary to remark that this type of studies are relevant to the Ecuador country, not only for study and research purposes, also for risk prevention in that prone zone, making links with local governments

who are responsible for operational activities in each territory. In addition, it is important establishing a route for the management and diffusion of information in an appropriate manner.

9. ACKNOWLEDGEMENTS

This study was supported by the Universidad de Tecnología Experimental Yachay under the guidance of Luis Pineda Ph.D. as advisor. The station data were provided by the Instituto Nacional de Meteorología e Hidrología (INAMHI). The information for climatological analysis and the satellite product CHIRPS were retrieved from the IRI website of Columbia University (<http://iri.columbia.edu/our-expertise/climate/tools>). The satellite imagery from GOES 13 was downloaded from the Comprehensive Large Array-Data Stewardship System (CLASS) developed by the National Oceanic and Atmospheric Administration (NOAA). The satellite precipitation data was retrieved from the Precipitation Process System developed by the National Aeronautics and Space Administration (NASA).

10. BIBLIOGRAPHY

- Bendix, A., Bendix, J. (2006). Heavy rainfall episodes in Ecuador during El Niño events and associated regional atmospheric circulation and SST patterns, *Adv. Geosci.*, 6 pp. 43-49, 10.5194/adgeo-6-43-2006.
- Bendix, J., Trache, K., Palacios, E., Rollenbeck, R., Goettlicher, D., Naus, T., & Bendix, A. (2011). El Niño meets La Niña – anomalous rainfall patterns in the “traditional” El Niño region of southern Ecuador. *Erdkunde*, 65(2), 151-167. doi: 10.3112/erdkunde.2011.02.04.
- CEPAL. (1983). Los desastres naturales de 1982–1983 en Bolivia, Ecuador y Perú. Naciones Unidas—Consejo Económico y Social—Comisión Económica Para América Latina. 227.
- Cruz, A., Cadier, E., Pourrut, P., Gomez, G., Rovere, O., Toscano, G., ... & Astudillo, L. (1977). Estudio hidro-meteorológico e hidrogeológico preliminar de las cuencas de los ríos Esmeraldas y del Norte ecuatoriano.
- Emck, P. (2007). A climatology of south Ecuador—with special focus on the major Andean ridge as Atlantic–Pacific climate divide Friedrich-Alexander-Universität. Erlangen-Nürnberg (PhD Thesis).
- Funk, C., Peterson, P., Landsfeld, M., Pedreros, D., Verdin, J., & Shukla, S. et al. (2015). The climate hazards infrared precipitation with stations—a new environmental record for monitoring extremes. *Scientific Data*, 2(1). doi: 10.1038/sdata.2015.66
- Goldberg, R., Tisnado M., G., & Scofield, R. (1987). Characteristics of extreme rainfall events in northwestern Peru during the 1982–1983 El Niño period. *Journal Of Geophysical Research*, 92(C13), 14225. doi: 10.1029/jc092ic13p14225

- Hengl T., Geuvelink, G.B.M. and Stein A. (2003). Comparison of kriging with external drift and regression-kriging. Technical note, ITC, Available on-line at [www.itc.nl/library/Academic output](http://www.itc.nl/library/Academic_output)
- Huffman, G. J., Adler, R. F., Bolvin, D. T., & Nelkin, E. J. (2010). The TRMM multi-satellite precipitation analysis (TMPA). In *Satellite rainfall applications for surface hydrology* (pp. 3-22). Springer, Dordrecht.
- Hughes, J., & Guttorp, P. (1994). Incorporating spatial dependence and atmospheric data in a model of precipitation. *Journal of Applied Meteorology*, 33(12):1503–1515.
- Kalnay, E., Kanamitsu, M., Kistler, R., Collins, W., Deaven, D., Gandin, L., ... & Zhu, Y. (1996). The NCEP/NCAR 40-year reanalysis project. *Bulletin of the American meteorological Society*, 77(3), 437-472.
- Li, M., & Shao, Q. (2010). An improved statistical approach to merge satellite rainfall estimates and raingauge data. *Journal Of Hydrology*, 385(1-4), 51-64. doi: 10.1016/j.jhydrol.2010.01.023
- Liu, C., E. J. Zipser, and S. W. Nesbitt, (2007). Global Distribution of Tropical Deep Convection: Different Perspectives from TRMM Infrared and Radar Data. *J. Climate*, 20, 489–503.
- Maddox, R. (1980). Mesoscale Convective Complexes. *Bulletin of The American Meteorological Society*, 61(11), 1374-1387. doi: 10.1175/1520-0477(1980)061<1374:mcc>2.0.co;2.
- Matheron, G. (1969). *Le krigeage universel (Universal kriging)*. vol. 1. Cahiers du Centre de Morphologie Mathematique, Ecole des Mines de Paris, Fontainebleau, 83pp.
- Mohr, K. I. and E. J. Zipser, 1996: Mesoscale Convective Systems Defined by Their 85-GHz Ice Scattering Signature: Size and Intensity Comparison over Tropical Oceans and Continents. *Mon. Wea. Rev.*, 124, 2417–2437.

- Morrison, H., S. A. Tessendorf, K. Ikeda, and G. Thompson, 2012: Sensitivity of a Simulated Midlatitude Squall Line to Parameterization of Raindrop Breakup. *Mon. Wea. Rev.*, 140, 2437–2460
- Nerini, D., Zulkafli, Z., Wang, L., Onof, C., Buytaert, W., Lavado-Casimiro, W., & Guyot, J. (2015). A Comparative Analysis of TRMM–Rain Gauge Data Merging Techniques at the Daily Time Scale for Distributed Rainfall–Runoff Modeling Applications. *Journal Of Hydrometeorology*, 16(5), 2153-2168. doi: 10.1175/jhm-d-14-0197.1
- Pineda, L., & Willems, P. (2018). Rainfall extremes, weather and climate drivers in complex terrain: A data-driven approach based on signal enhancement methods and EV modeling. *Journal of hydrology*, 563, 283-302.
- Pineda, L., & Willems, P. (2016). Multisite Downscaling of Seasonal Predictions to Daily Rainfall Characteristics over Pacific–Andean River Basins in Ecuador and Peru Using a Nonhomogeneous Hidden Markov Model. *Journal Of Hydrometeorology*, 17(2), 481-498. doi: 10.1175/jhm-d-15-0040.1
- Pourrut, P. (1995). El agua en el Ecuador, clima, precipitaciones, escorrentía (p. 14). Quito: Colegio de Geógrafos del Ecuador.
- Rasmusson, E. M., & Carpenter, T. H. (1982). Variations in tropical sea surface temperature and surface wind fields associated with the Southern Oscillation/El Niño. *Monthly Weather Review*, 110(5), 354-384.
- Rossel, F., Cadier, E. (2009). El Niño and prediction of anomalous monthly rainfalls in Ecuador. *Hydrol. Processes*, 23, 3253–3260, doi:<https://doi.org/10.1002/hyp.7401>.
- Silverman, B (1998). Density estimation for statistics and data analysis. *Monographs on Statistics and Applied Probability*, Vol 26, Chapman & Hall, 175 pp.

UCAR/COMET, U. (1997). Mesoscale convective systems: Squall lines and Bow Echoes. Retrieved 20 September 2019, from <https://www.meted.ucar.edu/convectn/mcs/mcsweb>

UCAR/COMET, U. (1997). Tropical mesoscale convective systems. Retrieved 01 January 2020, from https://www.meted.ucar.edu/tropical/synoptic/trop_MCS

Unidata, (2019). Integrated Data Viewer (IDV) version 5.6 [software]. Boulder, CO: UCAR/Unidata. (<http://doi.org/10.5065/D6RN35XM>)

Viterbi, J. (1967). Error bounds for convolutional codes and an asymptotically optimum decoding algorithm. *IEEE Transactions on Information Theory*, 13(2):260–269.

Waylen, P. R., & Caviedes, C. N. (1986). El Niño and annual floods on the north Peruvian littoral. *Journal of Hydrology*, 89(1-2), 141-156.

Zou, X., Qin, Z., & Zheng, Y. (2015). Improved Tropical Storm Forecasts with GOES-13/15 Imager Radiance Assimilation and Asymmetric Vortex Initialization in HWRF. *Monthly Weather Review*, 143(7), 2485-2505. doi: 10.1175/mwr-d-14-00223.1

11. ANNEXES

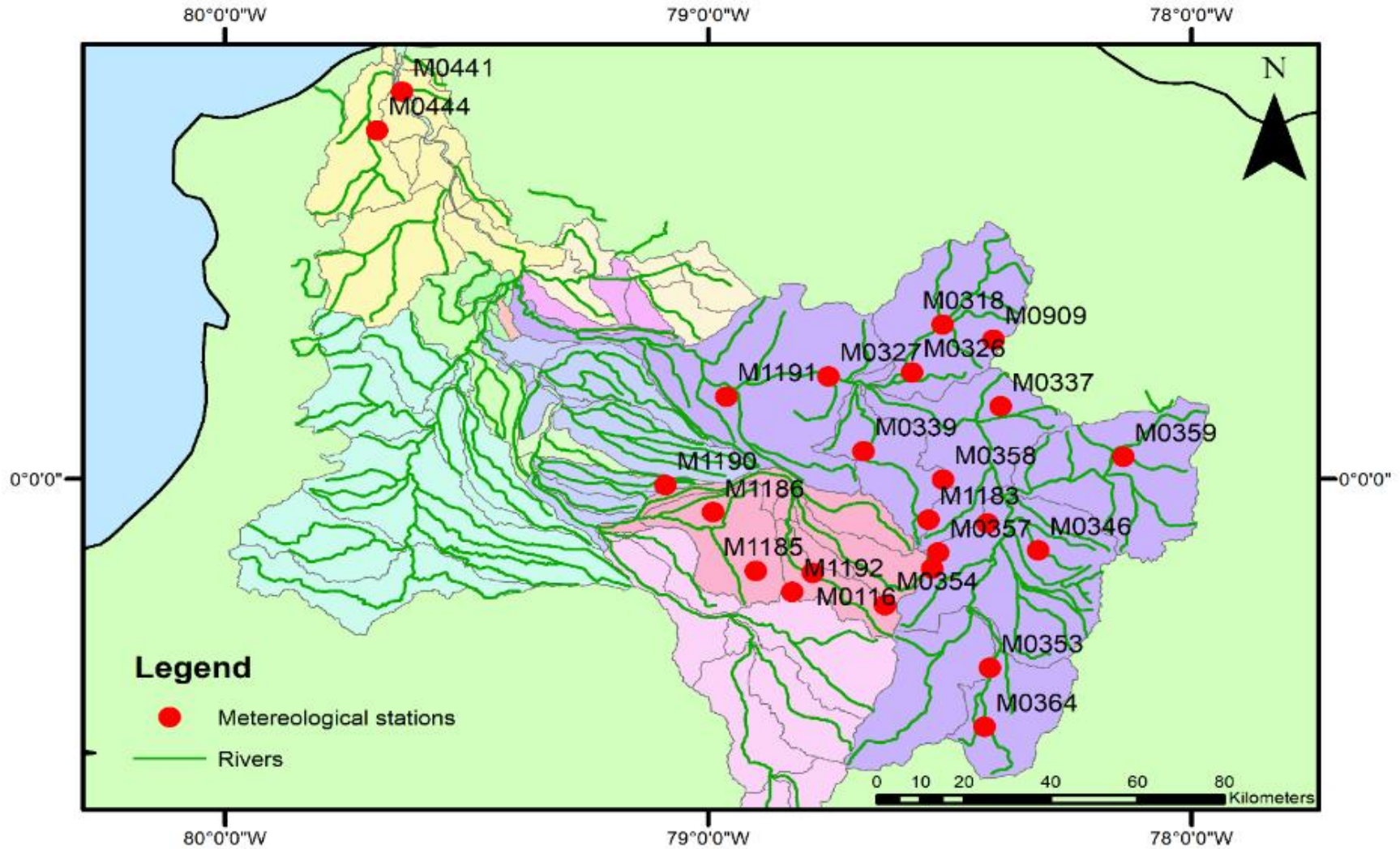


Figure A1. Esmeraldas river basin with meteorological stations network (red points) used to compute hietograms of precipitation (mm) in the event day.

Outlet Rio Esmeraldas Basin

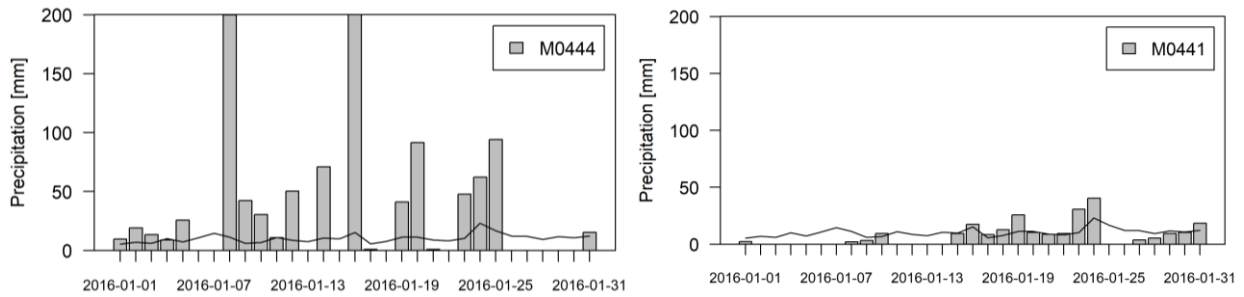


Figure A2. Hietograms of precipitation (mm) in January 2016 for outlet Rio Esmeraldas basin. Long-term mean for January (Black line) for the period (1985-2018).

Rio Blanco Basin

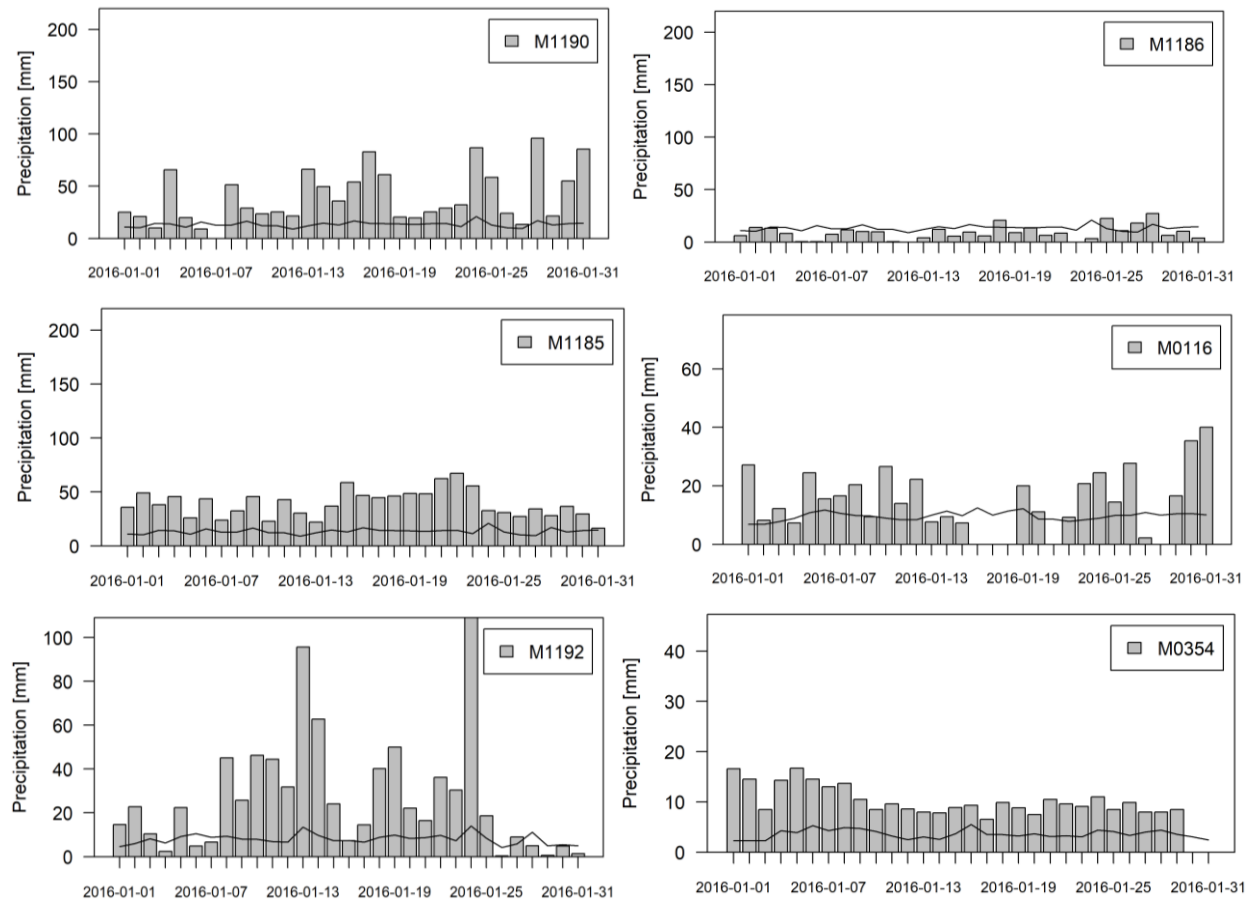


Figure A3. Hietograms of precipitation (mm) in January 2016 for Rio Blanco basin. Long-term mean for January (Black line) for the period (1985-2018).

Rio Guayllabamba North Basin

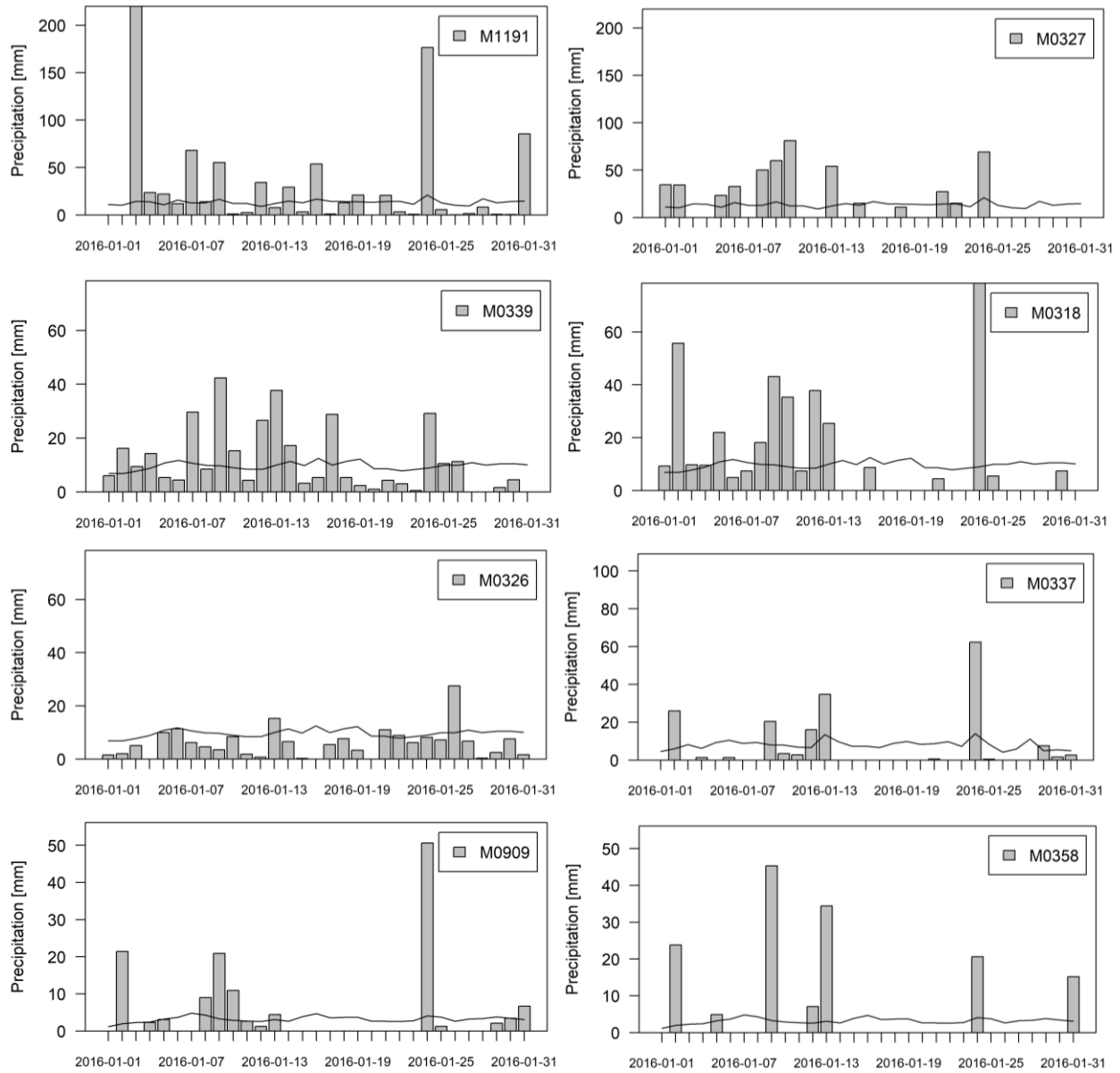


Figure A4. Hietograms of precipitation (mm) in January 2016 for outlet Rio Guayllabamba North basin. Long-term mean for January (Black line) for the period (1985-2018).

Rio Guayllabamba southeast Basin

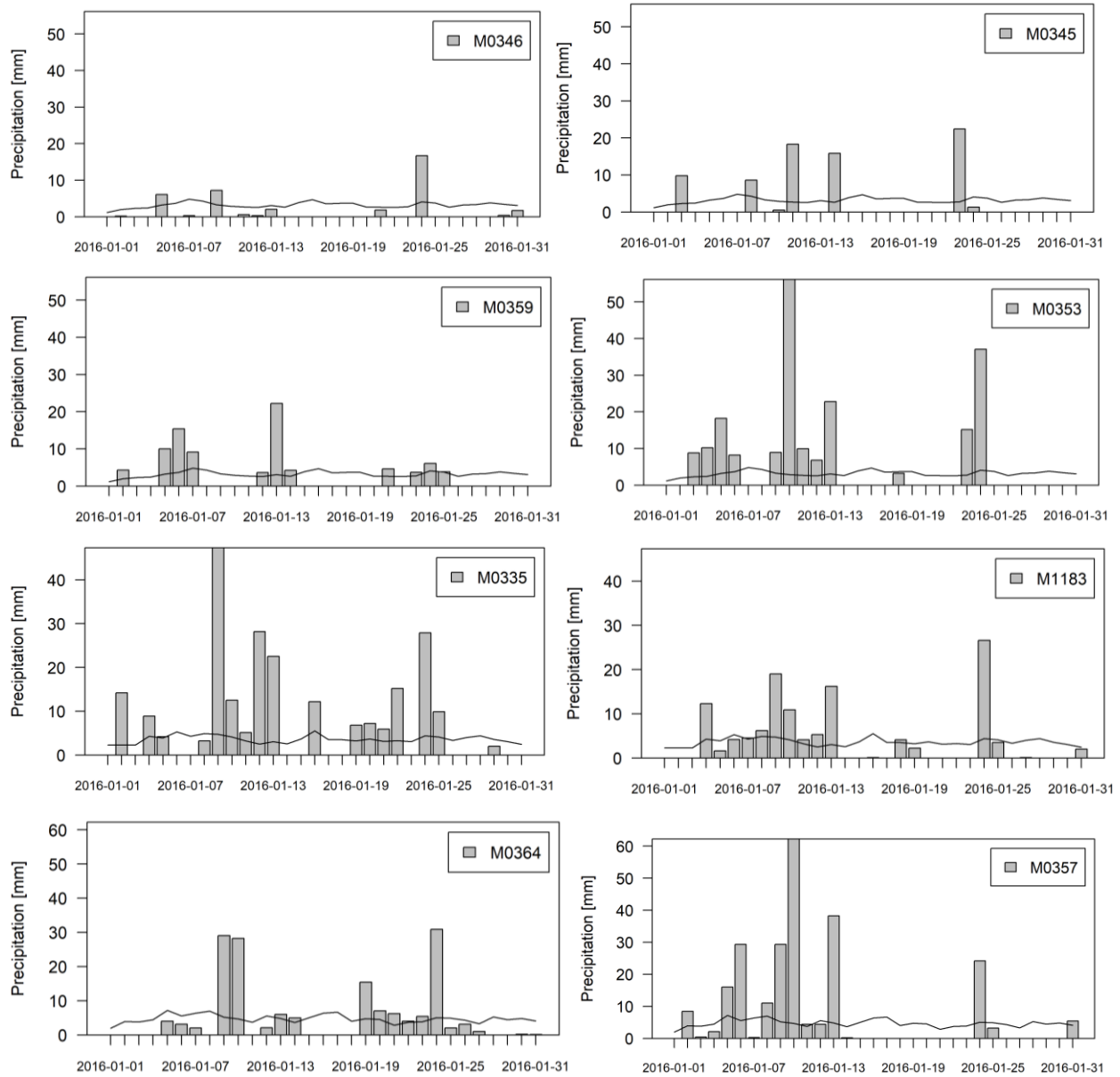


Figure A5. Histograms of precipitation (mm) in January 2016 for outlet Rio Guayllabamba southeast basin. Long-term mean for January (Black line) for the period (1985-2018).